J. Fluid Mech. (1987), *vol.* 176, *pp.* 483–520
Printed in Great Britain

The reflection of a plane shock wave over a double wedge

By G. BEN-DOR,
Department of Mechanical Engineering, Ben-Gurion University of the Negev, Beer Sheva, Israel

J. M. DEWEY
Department of Physics, University of Victoria, Victoria, British Columbia, Canada

AND K. TAKAYAMA
Institute of High Speed Mechanics, Tohoku University, Sendai, Japan

(Received 30 September 1985 and in revised form 29 July 1986)

An analysis is presented of the shock-wave configurations which will occur when a plane shock is incident on a double wedge for which the second wedge may have a greater (concave case) or a smaller (convex case) inclination than the first wedge. It is shown that seven different reflection processes may be expected depending on the Mach number of the incident shock M_1 and the two wedge angles θ_w^1 and θ_w^2. These processes may be defined by seven regions in the (θ_w^1, θ_w^2)-plane, for a given value of M_1. Each of the seven processes has been verified by sequences of shadowgraph and schlieren photographs.

A shock-polar analysis of each of the seven processes has provided information about the pressure changes and the wave structures which develop immediately behind the main reflections along the wedge surfaces. These wave structures have been verified experimentally, and two types have been observed: one normal to the reflecting surface, and the other in the form of a regular reflection. The criteria to determine which of these configurations will occur have not yet been established.

It is believed that the present study will be of value in predicting the loading of shock waves on structures, and may lead to a better understanding of shock reflections from concave and convex cylindrical surfaces.

1. Introduction

When a planar shock wave encounters a sharp compressive corner, such as the leading edge of a wedge, two different types of reflection may occur: regular reflection RR (figure 1*a*) or Mach reflection MR (figure 1*b*). Regular reflection consists of two shock waves, the incident shock i and the reflected shock r, which coincide on the wedge at the reflection point G. Mach reflection consists of four discontinuities, the incident shock i, the reflected shock r, the Mach stem m and the slipstream s, which coincide at the triple point T. Over a plane wedge the triple point moves along a straight line making an angle χ with the wedge surface. The Mach stem is usually curved.

For a given gas, the type of reflection which will occur depends on the strength of the incident shock, defined by the Mach number M_1, and on the wedge angle θ_w.

If a frame of reference is attached to the reflection point of a regular reflection or

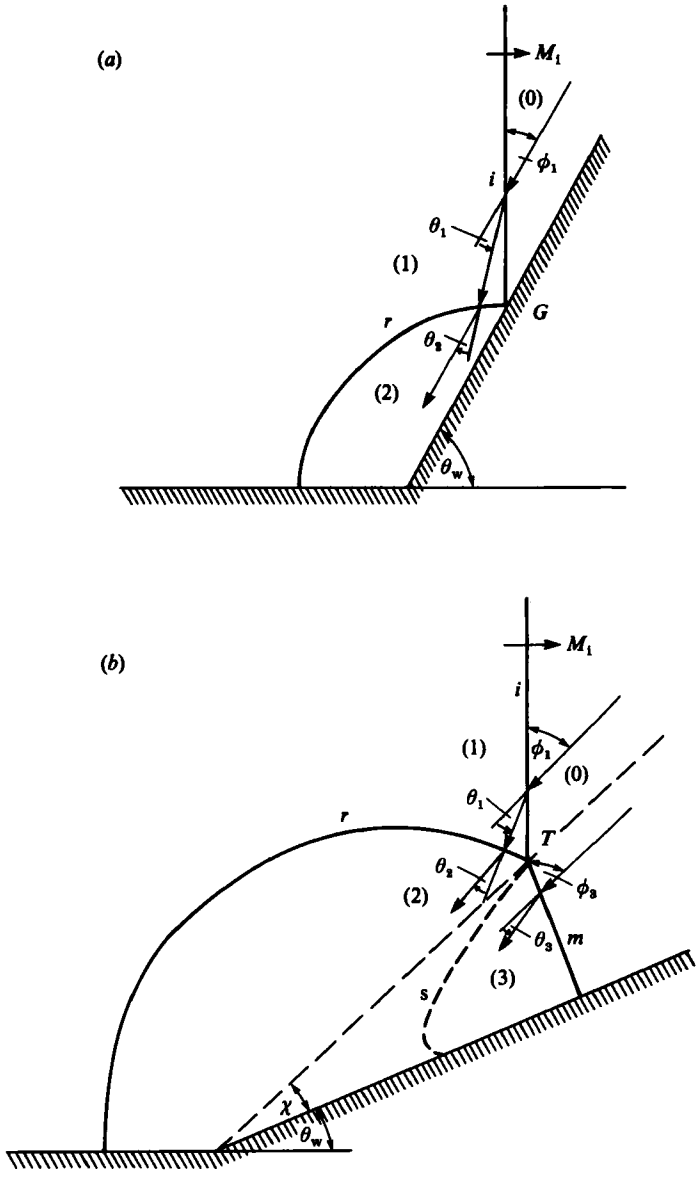

FIGURE 1. Schematic illustration of (*a*) regular reflection, and (*b*) Mach reflection, i, incident shock wave; r, reflected shock wave; m, Mach stem; s, slipstream; G, reflection point; T, triple point; θ_w, reflecting wedge angle; χ, triple point trajectory angle; ϕ, angle of incidence; θ, angle of deflection; (0)–(3), thermodynamic states.

the triple point of a Mach reflection, then the non-stationary regular or Mach reflection becomes pseudo-steady (Jones, Martin & Thornhill 1951), and the shock waves i, r and m can be treated using steady-flow theory. By considering these shock waves separately and using oblique-shock-wave relations with appropriate boundary conditions the equations of motion for regular and Mach reflection can be derived (Ben-Dor 1978).

In the case of an inviscid regular reflection (figure 1*a*) when the frame of reference

is attached to the reflection point, the flow in state (0) moves towards the reflection in a direction parallel to the wedge surface and at an angle of incidence ϕ_1 to the incident shock. On passing through the incident shock wave the flow is deflected towards the wedge surface by an angle θ_1. The flow then passes through the reflected shock wave which deflects it back by an angle θ_2 to become again parallel to the wedge surface. Therefore, the boundary condition for a regular reflection is:

$$\theta_1 - \theta_2 = 0. \tag{1}$$

Thus the flow directions in states (0), (1) and (2) with respect to the trajectory of the reflection point, G, are:

$$\theta_0^G = 0, \quad \theta_1^G = \theta_1, \quad \text{and} \quad \theta_2^G = \theta_1 - \theta_2 = 0, \tag{2}$$

respectively, where superscript G designates that θ is measured with respect to the direction defined by the trajectory of G.

In the case of Mach reflection (figure 1*b*) when the frame of reference is attached to the triple point T, the flow in state (0) moves towards the reflection in a direction parallel to the triple-point trajectory. The flow above the triple-point trajectory approaches the incident shock wave at an angle of incidence ϕ_1. On passing through the incident shock the flow is deflected towards the wedge by an angle of θ_1. It then passes through the reflected shock which deflects it back by an angle θ_2, parallel to the slipstream. Below the triple-point trajectory the flow approaches the Mach stem at an angle of incidence ϕ_3, and is deflected towards the wedge by an angle θ_3, also parallel to the slipstream. Since the flows in states (2) and (3) are parallel and separated by a slipstream across which there is no change of static pressure, the boundary conditions for the Mach reflection are:

$$\theta_1 - \theta_2 = \theta_3, \quad \text{and} \quad P_2 = P_3, \tag{3}$$

where P is the static pressure. Thus the flow directions in states (0), (1), (2), and (3) with respect to the trajectory of the triple point, T, are:

$$\theta_0^T = 0; \quad \theta_1^T = \theta_1; \tag{4}$$

$$\theta_2^T = \theta_1 - \theta_2, \quad \text{and} \quad \theta_3^T = \theta_3.$$

Equations (3) and (4) give;

$$\theta_2^T = \theta_3^T. \tag{5}$$

Kawamura & Saito (1956) suggested that, since the boundary conditions (1) and (3) are in terms of the flow deflection angles, θ, and pressures, P, the relationship between P and θ may be of importance in understanding shock reflection phenomena. The graphical representation of the relationship between the pressure ratio, P/P_0, across an oblique shock and the angle, θ, through which the flow is deflected by the shock for a fixed value of the Mach number of the incident flow, M_0, is called a pressure-deflection shock polar.

Figure 2(*a*) represents the (P, θ) polar solution of a regular reflection. All the flow deflection angles, θ^G, are measured with respect to the trajectory of the reflection point G (see figure 1*a*). State (0) is represented by the origin, where $P = P_0$ and $\theta_0^G = 0$. The locus of all the flow states which can be obtained from state (0) by passing through any oblique shock wave is represented by the I polar. Consequently, state (1) of a regular reflection is represented on the I polar by the point $P = P_1$ and $\theta^G = \theta_1^G$. The R polar is the locus of all the flow states which can be obtained from state (1)

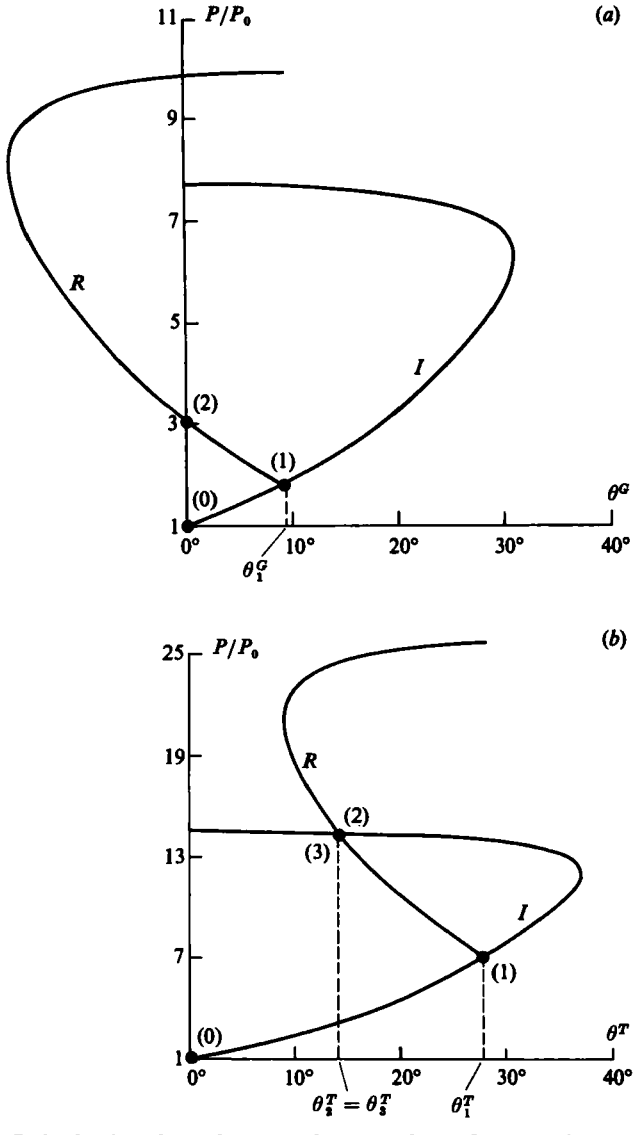

FIGURE 2. (P, θ) shock-polar solutions of (*a*) regular reflection ($M_1 = 1.3, \theta_w = 60°$) and (*b*) Mach reflection ($M_1 = 2.5, \theta_w = 40°, \chi = 5.29°$). The flow states are labelled (0) ahead of the incident shock wave, (1) behind the incident shock wave, (2) behind the reflected shock wave and (3) behind the Mach stem. R is the reflected shock polar, and I the polar for both the incident and Mach-stem shocks which encounter the same incident flow in a pseudo-steady frame of reference.

by passing through any oblique shock. Consequently, state (2) which is obtained from state (1) by passing through the reflected shock wave is on the R polar. The boundary condition (2) implies that $\theta_2^G = 0$, therefore, state (2) is represented by the point where the R polar intersects the P-axis (i.e. $\theta^G = 0$) as illustrated in figure 2(*a*).

Figure 2(*b*) represents the (P, θ) polar solution of a Mach reflection. All the deflection angles are measured with respect to the trajectory of the triple point (see figure 1*b*). Again, state (1) behind the incident shock lies on the I polar and is the origin of the R polar, and state (2), behind the reflected shock lies on the R polar.

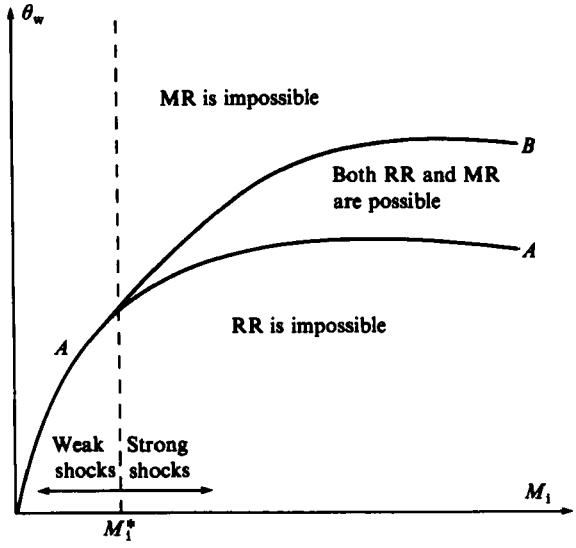

FIGURE 3. Regions of possible types of reflection in the (M_1, θ_w)-plane. M_1 is the incident-shock-wave Mach number, θ_w the reflecting wedge angle, and M_1^* the limiting Mach number separating weak and strong shocks. For $\gamma = \frac{7}{5}$, $M_1^* = 1.4565$.

State (3) behind the Mach stem also lies on the I polar. Since the pressures and the flow directions with respect to the triple-point trajectory in states (2) and (3) are equal, states (2) and (3) are represented by the intersection of the I and R polars.

Figure 3 illustrates the regions in the (M_1, θ_w)-plane in which the different types of reflection are possible or impossible. The regions are separated by curves A and B. Curve A describes the 'detachment' criterion of von Neumann (1963), and curve B the 'mechanical equilibrium' criterion of Henderson & Lozzi (1975). Hornung, Oertel and Sandeman (1979) used a 'corner signal' concept to show that transition from regular to Mach reflection is best defined by the 'sonic' criterion, namely the condition when the signal speed behind the reflected shock equals that of the reflection point. The 'sonic' criterion is very close to the detachment criterion, particularly for strong shocks.

For a given gas (i.e. value of the specific heat ratio, γ) there is a certain value of incident shock Mach number, M_1^*, below which the 'mechanical equilibrium' criterion does not exist. Henderson & Woolmington (1983) have shown that for a diatomic gas, $\gamma = \frac{7}{5}$, $M_1^* = 1.4565$ and for a monatomic gas, $\gamma = \frac{5}{3}$, $M_1^* = 1.5487$. Incident shock waves with Mach numbers in the range $M_1 < M_1^*$ are called weak shocks and those in the range $M_1 > M_1^*$ are called strong shocks. Figure 3 indicates that for weak shocks there is one region in which regular reflection is theoretically impossible ($\theta_w < \theta_w^{det}$) and another region in which Mach reflection is theoretically impossible ($\theta_w > \theta_w^{det}$). The regions are separated by the detachment transition line $\theta_w = \theta_w^{det}$. However, for the strong shocks there is a region, $\theta_w < \theta_w^{det}$, in which regular reflection is theoretically impossible; a region, $\theta_w > \theta_w^{m.e.}$, in which Mach reflection is theoretically impossible, and an additional region, $\theta_w^{det} < \theta_w < \theta_w^{m.e.}$, in which both regular and Mach reflection are theoretically possible. Dewey & McMillin (1985) have shown that the assumption of pseudo-stationarity may not be valid for weak Mach reflections and that realistic shock polars cannot be drawn for this region.

In the case of truly unsteady flows, i.e. flows which cannot be made pseudo-steady

by a simple coordinate transformation, the wedge angle at which transition from regular to Mach reflection occurs depends on the geometry of the process itself. For example, the MR→RR transition over concave cylinders occurs at wedge angles greater than those predicted by the 'mechanical equilibrium' transition line, and the RR→MR transition over convex cylinders occurs at wedge angles smaller than those predicted by the 'detachment' transition line. For both cases the transition angle also depends on the initial angle of incidence and the radius of curvature of the cylindrical wedges. Details of these reflection phenomena are described by Heilig (1969), Ben-Dor, Takayama & Kawauchi (1980), Itoh, Okazaki & Itaya (1981) and Dewey *et al.* (1983). To the best of our knowledge, no shock-wave phenomenon has been recorded yet, in which the RR $\rightleftarrows$ MR transition occurs at wedge angles in the range $\theta_{\mathrm{w}}^{\mathrm{det}} < \theta_{\mathrm{w}}^{\mathrm{tr}} < \theta_{\mathrm{w}}^{\mathrm{m.e.}}$.

A suggested approach to the study of shock-wave reflections from concave and convex cylindrical surfaces is a consideration of the reflection from a double wedge with a single increase or decrease of the wedge angle. In the present paper, seven different shock configurations resulting from the reflection of a planar shock wave over a concave or a convex double wedge are identified and investigated analytically and experimentally.

A study of the reflection process over three of the seven possible double-wedge combinations was conducted by Ginzburg & Markov (1975). However, it will be shown that some of the schematic drawings in their paper, illustrating the wave configurations, are incorrect. This is probably due to the poor resolution of their photographic method. Some of their schematic drawings show confluence points of four shocks, which are known to be theoretically impossible (Courant & Friedrichs 1948), and others fail to observe the details of the wave structure.

Two of the possible Mach configurations over a concave double wedge have been studied by Matsuo, Aoki, Hirahara & Kondoh (private communication 1985) and their observations appear to be in agreement with the results presented here.

2. Analysis

The analysis presented below establishes all the reflection processes and final shock configurations that are possible over any double-plane-wedge combination. A compressive and an expansive double wedge are illustrated in figures 4(*a*) and 4(*b*), respectively. The slopes of the first and second wedges are θ_{w}^{1} and θ_{w}^{2}, respectively, and the slope of the second wedge with respect to the first is

$$\Delta\theta_{\mathrm{w}} = \theta_{\mathrm{w}}^{2} - \theta_{\mathrm{w}}^{1}. \tag{6}$$

The reflection over a double wedge depends on three parameters: the incident-shock-wave Mach number M_1, and the first and second wedge angles θ_{w}^{1} and θ_{w}^{2}.

In the following analysis it will be assumed that: (i) the flow is two dimensional; (ii) the gas is perfect ($p = \rho RT$) and ideal ($\mu = 0, k = 0$); (iii) the flow over the first wedge is pseudo-steady; (iv) the flow over the second wedge asymptotically approaches a pseudo-steady situation; (v) the regular $\rightleftarrows$ Mach reflection transition follows the 'detachment' criterion, and (vi) the incident shock waves are weak enough so that if the reflection over the first wedge is a Mach-type reflection, it is a single Mach reflection. Further assumptions concerning the Mach stems are given subsequently.

For a given shock-wave Mach number there is an appropriate 'detachment' wedge angle, $\theta_{\mathrm{w}}^{\mathrm{det}}$. If $\theta_{\mathrm{w}}^{1} < \theta_{\mathrm{w}}^{\mathrm{det}}$ the shock wave reflects from the first wedge as a Mach

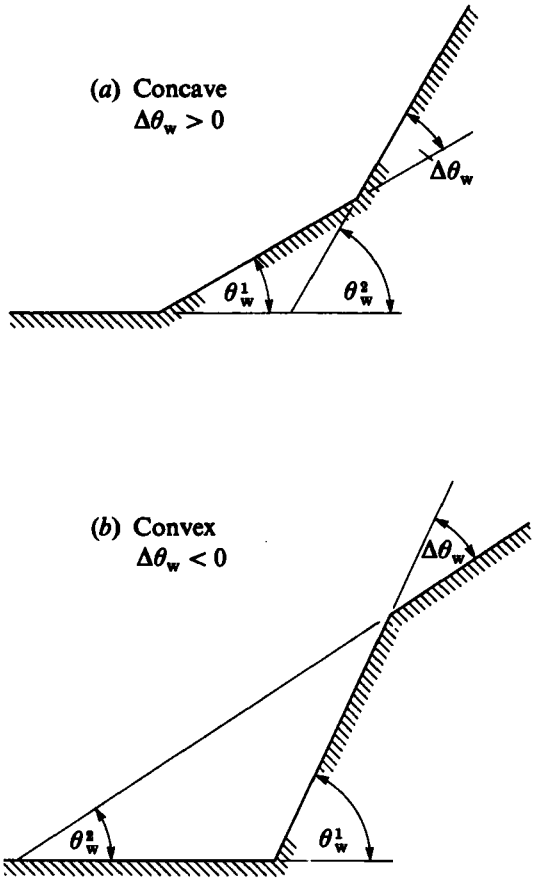

FIGURE 4. Two double wedge configurations, (*a*) concave and (*b*) convex. θ_w^1 is the first wedge angle, $\Delta\theta_w$ the second wedge angle with respect to the first wedge, and θ_w^2 the second wedge angle.

reflection, and if $\theta_w^1 > \theta_w^{det}$ it reflects over the first wedge as a regular reflection. The Mach or the regular reflection propagates up the wedge until it encounters the leading edge of the second wedge. If the incident shock wave has reflected as a Mach reflection over the first wedge, then the Mach stem of this reflection encounters the second wedge and reflects from it either as a Mach or as a regular reflection depending upon the size of the differential wedge angle, $\Delta\theta_w$, and the Mach number of the Mach stem, M_m.

In the following analysis it will be assumed that the Mach stem is straight and perpendicular to the wedge surface so that

$$M_m = M_1 \frac{\cos\chi_1}{\cos(\theta_w^1 + \chi_1)}, \tag{7}$$

where χ_1 is the first triple-point trajectory angle (Ben-Dor 1980). Thus $M_m > M_1$, but the difference in Mach number is not large and it will therefore be assumed that

$$\theta_w^{det}|_{M_m} \approx \theta_w^{det}|_{M_1}. \tag{8}$$

For example, for $M_1 = 2.5$ and $\theta_w^1 = 20°$ the Mach reflection solution results in $\chi_1 = 12.88°$, thus $M_m = 2.902$. The corresponding detachment wedge angles for M_1

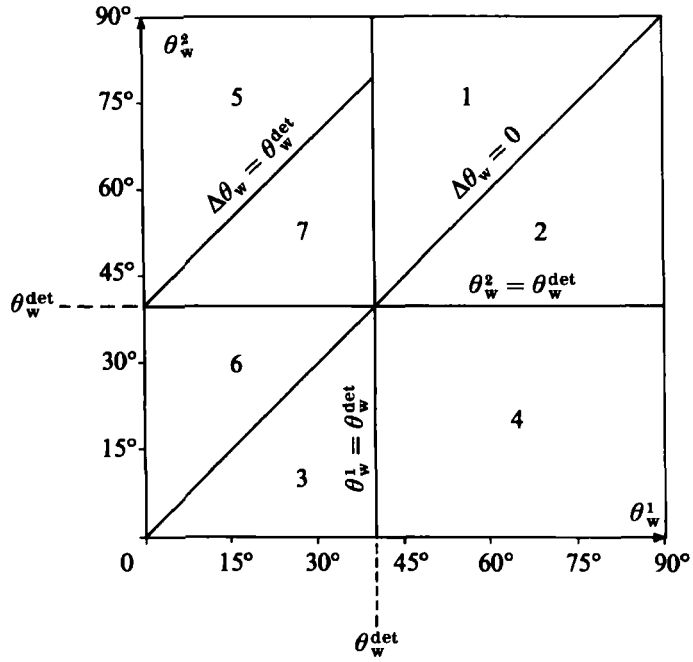

FIGURE 5. The seven regions in the (θ_w^1, θ_w^2)-plane which identify the different reflection processes of a shock wave over a double wedge. θ_w^1 is the first wedge angle, $\Delta\theta_w$ the second wedge angle with respect to the first wedge, θ_w^2 the second wedge angle, and θ_w^{det} the detachment wedge angle corresponding to the incident shock wave Mach number, M_i. The reflection processes in each region are given in table 1.

and M_m are 50.77° and 50.72°, respectively. Similarly, for $M_i = 1.775$ and $\theta_w^1 = 20°$, one obtains $\chi_1 = 16.17°$ and $M_m = 2.112$. For this case the corresponding detachment wedge angles are 50.22 and 50.68. These two examples indicate that although the difference between the incident-shock-wave Mach number and the Mach-stem Mach number is about 15 %, the difference in the detachment angle for these shocks is only a fraction of a degree. Using the assumption of (8), it may be concluded that the Mach stem of the first Mach reflection reflects from the second wedge as a Mach reflection if, $\Delta\theta_w < \theta_w^{det}$, and as a regular reflection if $\Delta\theta_w > \theta_w^{det}$.

The lines $\theta_w^1 = \theta_w^{det}$, $\theta_w^2 = \theta_w^{det}$, $\Delta\theta_w = 0$ and $\Delta\theta_w = \theta_w^{det}$ are all drawn in the (θ_w^1, θ_w^2)-plane shown in figure 5. These boundary lines define seven regions with different reflection processes. Those regions above the diagonal, $\Delta\theta_w = 0$, are for a concave double wedge, and those below the diagonal are for a convex wedge. The reflection process in each region and a shock-polar solution which gives information about the pressure changes produced by the reflection process are presented, beginning with the simplest case and ending with the most complicated.

The input data for the analysis were the incident-shock-wave Mach number, M_i and the double-wedge geometry, θ_w^1 and $\Delta\theta_w$. The analysis used the two-shock and the three-shock theories of von Neumann (1963) to determine the shock-wave angles and the thermodynamic properties behind the shocks for each reflection. The flow properties obtained from the solution were used to draw the shock polars shown subsequently, which are accurately drawn to scale.

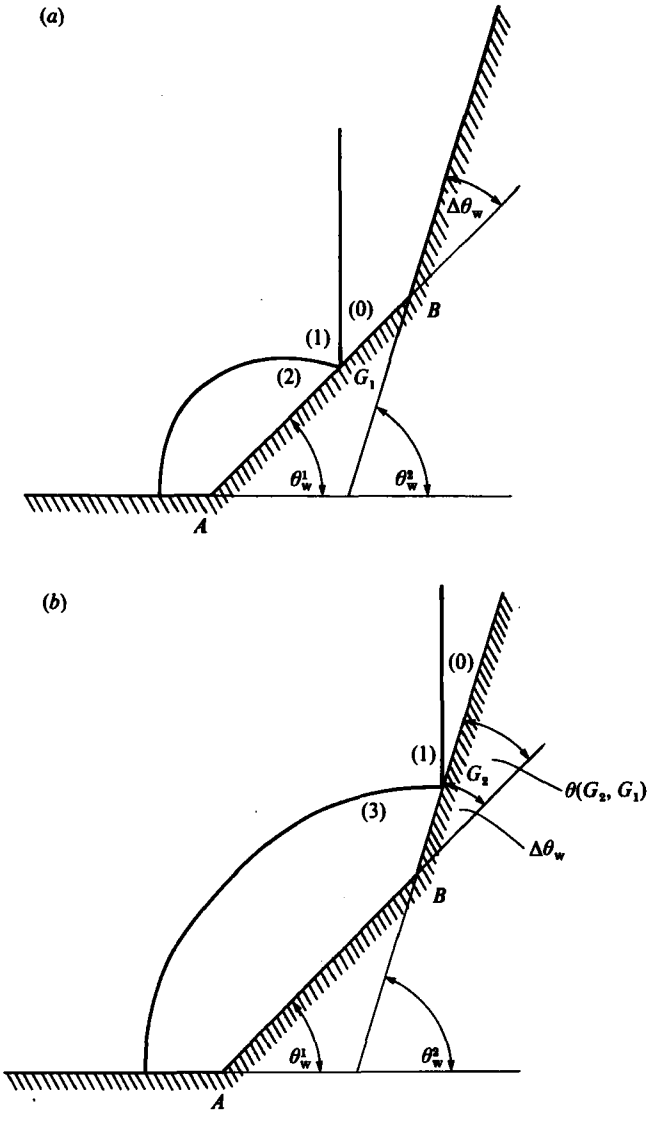

FIGURE 6. Schematic illustration of the shock wave reflections over (*a*) the first and (*b*) the second wedge for region 1 of figure 5.

Region 1

In this region $\Delta\theta_w > 0$; $\theta_w^1 > \theta_w^{det}$, and $\theta_w^2 > \theta_w^{det}$, and the reflection process is shown schematically in figure 6, with regular reflection over both wedges, but with different wave angles. The regular reflections can be considered by attaching frames of reference to the reflection points G_1 or G_2, as appropriate.

In order to combine the shock polars of the two regular reflections on a single plot in the (P, θ^{G_1})-plane it is necessary to know the direction of G_2 with respect to G_1, namely:

$$\theta(G_2, G_1) = \theta_w^2 - \theta_w^1 = \Delta\theta_w. \tag{9}$$

A shock-polar solution for a typical reflection process in region 1 is shown in figure 7 for initial conditions of $M_1 = 1.3$, $\theta_w^1 = 47°$ and $\Delta\theta_w = 13°$.

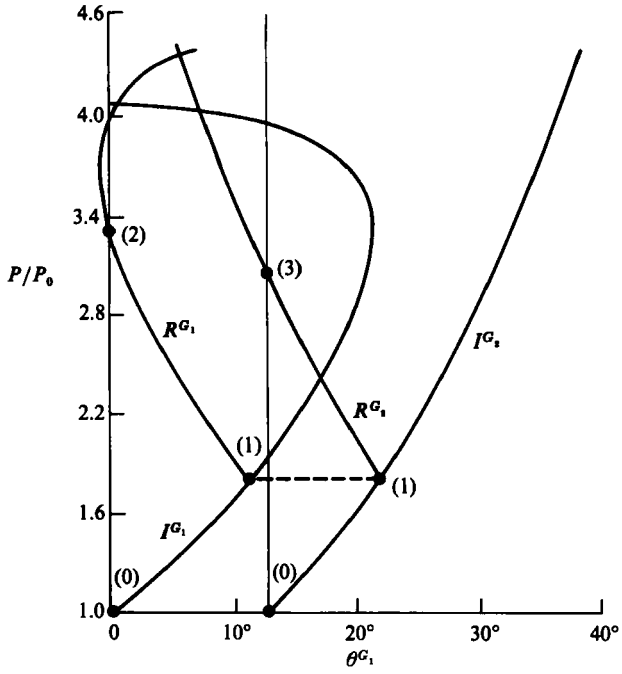

FIGURE 7. The shock-polar solution of the shock-wave reflection process for region 1. The polars are drawn accurately for an incident shock with Mach number $M_i = 1.3$, and a double concave wedge with inclinations $\theta_w^1 = 47°$ and $\theta_w^2 = 60°$. I^{G_1}, R^{G_1} and I^{G_2}, R^{G_2} are the incident and reflected shock polars for the pseudo-steady regular reflections over the first and second wedges, respectively.

The I^{G_1} and R^{G_1} polars represent the regular reflection over the first wedge. Since the solution of the reflection over the second wedge is in a frame of reference rotated by the angle $\theta(G_2, G_1)$ with respect to the original frame of reference, the origin of the I^{G_2} and R^{G_2} shock-polars combination is located at $\theta^{G_1} = \theta(G_2, G_1) = \Delta\theta_w$. Since $\theta_w^2 > \theta_w^1$, the velocity of G_2 is greater than that of G_1, and so the I^{G_2} polar is larger than the I^{G_1} polar. The pressure behind the incident shock is the same for both reflections and so the points representing state (1), i.e. the origins of the R^{G_1} and R^{G_2} polars, have the same ordinates in the (P, θ^{G_1})-plane.

The pressure P_2 in state (2) behind the reflected shock over the first wedge is given by the intersection of the R^{G_1} polar with the pressure axis, i.e. point (2) in figure 7, and the pressure P_3 in state (3) behind the reflected shock over the second wedge is given by the intersection of the R^{G_2} polar with the $\Delta\theta_w$ ordinate, i.e. point (3). In general $P_2 \neq P_3$, and as the incident shock moves from the first to the second wedge there will be a sudden change of pressure.

According to Henderson & Lozzi (1975), 'If a pressure discontinuity occurs during transition then an unsteady wave of finite amplitude or a finite amplitude band of waves will be generated in the flow'. We may therefore expect that the reflection point on the second wedge will be followed by either compression waves (or a shock wave) or expansion waves depending upon whether the transition causes a sudden pressure decrease or increase.

Figure 8 shows the theoretical pressure ratio behind the reflection point of a regular reflection as a function of the reflecting wedge angle θ_w for a given incident shock Mach number $M_i = 1.3$. The pressure ratio P_2/P_0 goes through a minimum at about $\theta_w = 60°$. Consequently, in the double-wedge reflection process now being considered

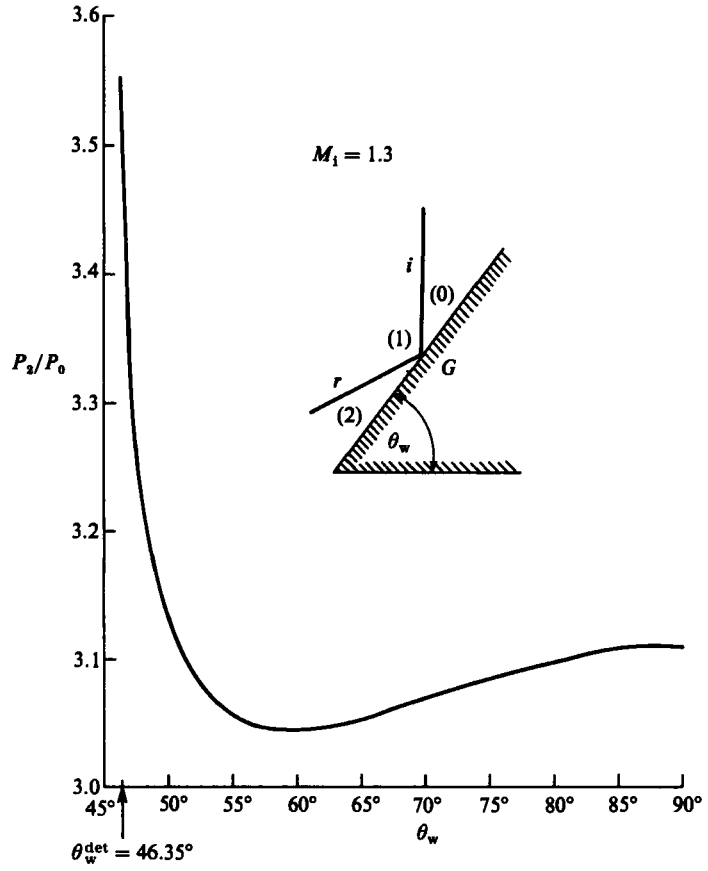

FIGURE 8. The ratio, P_2/P_0, of the pressures behind and ahead of the reflection point of a regular reflection as a function of the reflecting wedge angle, θ_w, for an incident-shock-wave Mach number $M_1 = 1.3$, calculated using two-shock theory.

three pressure-change behaviours are possible. If, in the example for $M_1 = 1.3$, $\theta_w^1 = 50°$ and $\theta_w^2 = 60°$ then at transition from the first to the second wedge the pressure behind the reflection point suddenly drops. However, if $\theta_w^1 = 60°$ and $\theta_w^2 = 85°$ then at transition the pressure behind the reflection point suddenly increases. There could also be a case for which there is no pressure change at transition e.g. $\theta_w^1 = 55°$ and $\theta_w^2 = 65.775°$. Thus, different flow patterns are to be expected behind the second reflection point according to these different pressure changes.

Region 2

In this region $\Delta\theta_w < 0$; $\theta_w^1 > \theta_w^{det}$, and $\theta_w^2 > \theta_w^{det}$, and the reflection process is shown schematically in figure 9. The reflection is regular over both wedges, and can be made pseudo-stationary by attaching frames of reference to the points of reflection G_1 and G_2. The direction of the second reflection point G_2 with respect to that of the first, G_1, is given by

$$\theta(G_2, G_1) = \Delta\theta_w. \tag{10}$$

and for a convex double wedge $\Delta\theta_w$ is negative.

A shock-polar solution for a typical reflection process in region 2 is shown in figure 10, for $M_1 = 1.3$, $\theta_w^1 = 60°$ and $\Delta\theta_w = -13°$.

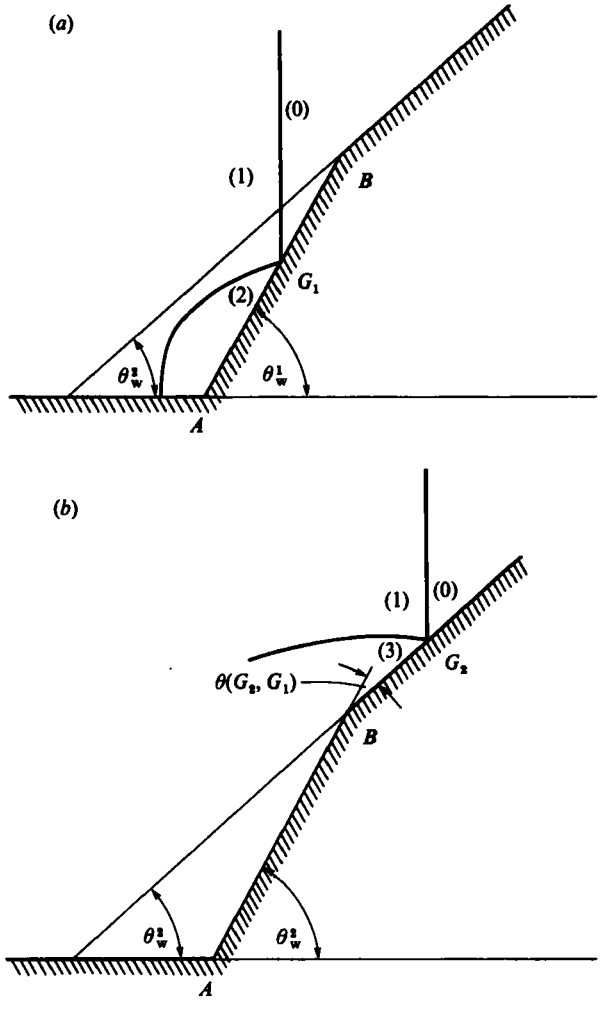

FIGURE 9. Schematic illustration of the shock-wave reflections over (*a*) the first and (*b*) the second wedge for region 2.

The I^{G_1}, R^{G_1} and I^{G_2}, R^{G_2} polars represent the solutions of the regular reflections over the first and second wedges, respectively, with the origin of I^{G_2} shifted by $\Delta\theta_w$ in the (P, θ^{G_1})-plane so that the I^{G_2} and R^{G_2} polars are now to the left of the I^{G_1} and R^{G_1} polars. The pressure in state (1), behind the incident shock is identical for both frames of reference, and the two shock-polar combinations are bridged by the constant pressure line P_1 which is dashed in figure 10.

The velocity of G_1 is greater than that of G_2 and so in the pseudo-steady frames of reference the velocity of the incident flow over the first wedge, $M_0^{G_1}$, is greater than that over the second, $M_0^{G_2}$. Therefore, the I^{G_1} polar is larger than the I^{G_2} polar. The polars again indicate that, in general, the pressure behind the reflected shock over the first wedge, P_2, will be different from the pressure behind the reflected shock over the second wedge, P_3, which should therefore be followed by either compression or expansion waves depending upon whether the pressure suddenly decreases or increases at transition from the first to the second wedge.

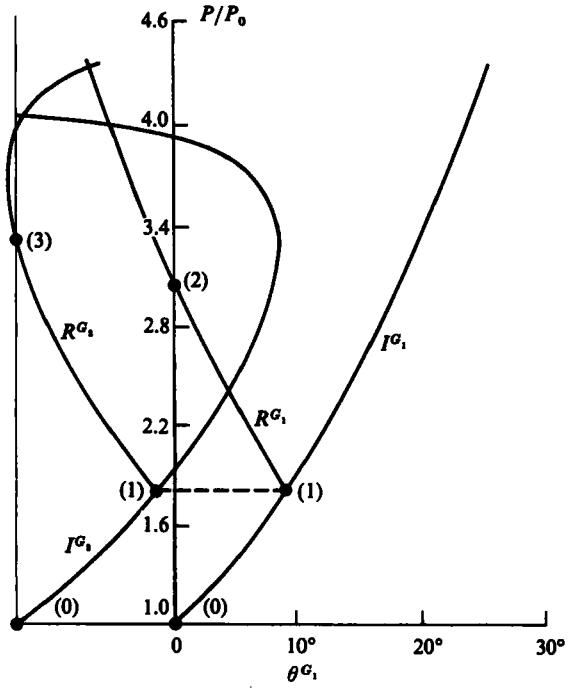

FIGURE 10. The shock-polar solution of the shock-wave reflection process for region 2. The polars are drawn accurately for an incident shock with Mach number $M_1 = 1.3$, and a double convex wedge with inclinations $\theta_w^1 = 60°$ and $\theta_w^2 = 47°$. I^{G_1}, R^{G_1} and I^{G_2}, R^{G_2} are the incident and reflected shock polars for the pseudo-steady regular reflections over the first and second wedges, respectively.

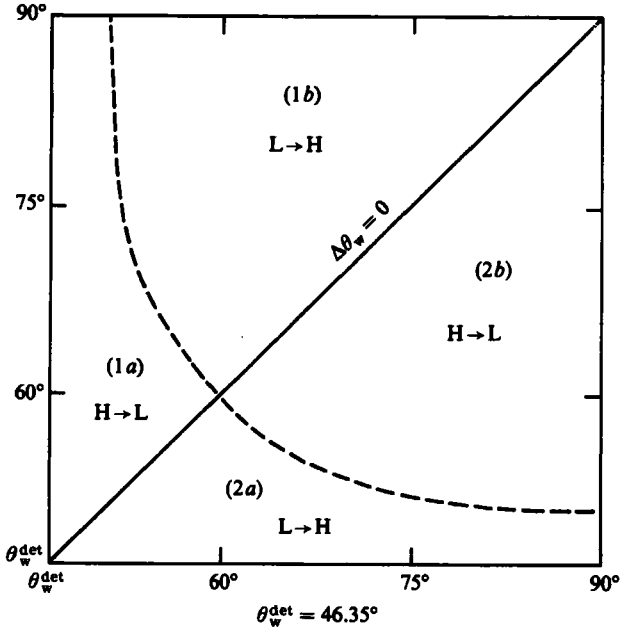

FIGURE 11. Subregions of the different regular to regular reflection processes in regions 1 and 2. In subregions $1a$ and $2b$ there will be a transition from high to low pressure behind the reflected shock (H→L), and in subregions $1b$ and $2a$, a transition from low to high pressure (L→H).

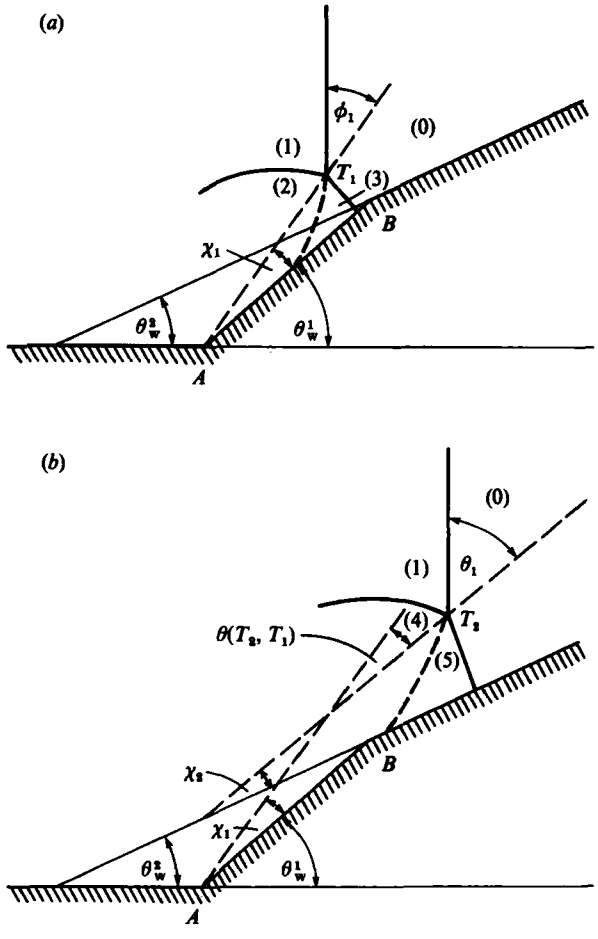

FIGURE 12. Schematic illustration of the shock-wave reflection process for region 3. (*a*) Mach reflection over the first wedge and (*b*) Mach reflection over the second wedge.

Figure 11 is an enlarged drawing of regions 1 and 2 of figure 5. The added dashed line divides each region into two subregions 1*a* and *b* and 2*a* and *b*. In subregions 1*a* and 2*b* the reflection process involves a transition from a high-pressure regular reflection to a low-pressure regular reflection (H→L) while in 1*b* and 2*a*, the transition is from a low-pressure regular to a high-pressure regular reflection (L→H). Therefore in subregions 1*a* and 2*b* it is expected that the reflection over the second wedge will be followed by a shock or compression wave, while in subregions 1*b* and 2*a* the second reflection is expected to be followed by an expansion wave. It is of interest to note that in region 1*a* the pressure behind the reflected shock may be expected to drop as the shock passes a compressive corner and in region 2*a* the pressure may be expected to increase around an expansive corner.

Region 3

In this region $\Delta\theta_w < 0$; $\theta_w^1 < \theta_w^{det}$, and $\theta_w^2 < \theta_w^{det}$, and the reflection process is shown schematically in figure 12. There is a Mach reflection over both wedges, but with different wave angles, and a non-stationary transition region. The initial and final Mach reflections can be made pseudo-stationary by attaching frames of reference to

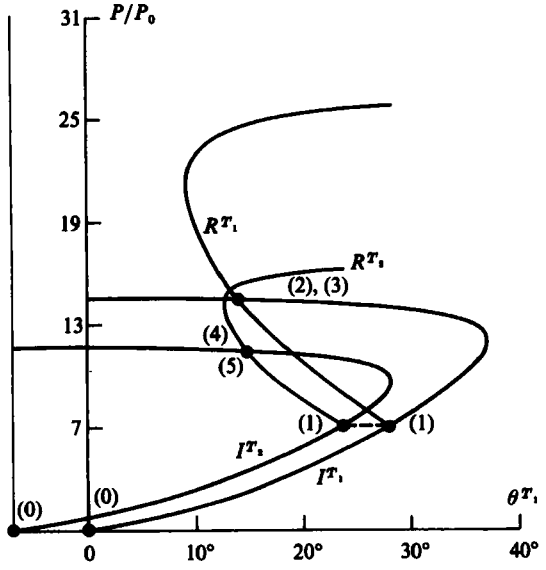

FIGURE 13. The shock-polar solution of the shock-wave reflection process in region 3. The polars are drawn accurately for an incident shock with Mach number $M_1 = 2.5$, and a double convex wedge with inclinations $\theta_w^1 = 60°$ and $\theta_w^2 = 47°$. I^{G_1}, R^{G_1} and I^{G_2}, R^{G_2} are the incident and reflected shock $\chi_2 = 8.27°$. I^{T_1}, R^{T_1} and I^{T_2}, R^{T_2} are the incident and reflected shock polars for the pseudo-steady Mach reflections over the first and second wedges, respectively. The polars are linked by a dashed line representing the constant pressure of state (1) behind the incident shock.

the triple points T_1 and T_2. The direction of T_2 with respect to the direction of the T_1, is given by

$$\theta(T_2, T_1) = -(-\Delta\theta_w + \chi_1 - \chi_2), \tag{11}$$

where χ_1 and χ_2 are the triple-point trajectory angles with respect to the two wedges.

A shock-polar solution for a typical reflection process in region 3 is shown in figure 13. The incident-shock-wave Mach number is $M_1 = 1.25$. It initially reflects as a Mach reflection over the first wedge for which $\theta_w^1 = 40°$ and $\chi_1 = 5.29$. $\Delta\theta_w = -10°$ and the Mach reflection over the second wedge for which $\theta_w^2 = 30°$, has a triple-point trajectory angle $\chi_2 = 8.27°$.

The I^{T_2} and R^{T_2} polars are plotted in the (P, θ^{T_1})-plane, with the origin of the I^{T_2} polar displaced by $(\Delta\theta_w - \chi_1 + \chi_2)$. Since the inclination of the second triple-point trajectory is less than that of the first, the velocity of T_2 is less than that of T_1 and the Mach number of the incident flow in the pseudo-steady frame of reference, $M_0^{T_2}$ will be less than that over the first wedge, $M_0^{T_1}$. The I^{T_2} polar is therefore smaller than the I^{T_1} polar. The two polars are again related by the pressure P_1 behind the incident shock, shown as a dashed line in the figure. It can be seen that the pressure behind the Mach stem over the second wedge, P_5, will be less than the pressure behind the Mach stem over the first wedge, P_3. Because the signal speed, i.e. the sound speed plus the particle velocity behind the Mach stem is greater than the speed of the Mach stem, any compression waves will overtake the Mach stem. It is expected, therefore, that after transition from the first to the second wedge, the Mach-stem shock initially will be stronger than that produced by an incident shock reflection from a single wedge with an inclination θ_w^2, but will asymptotically approach that value.

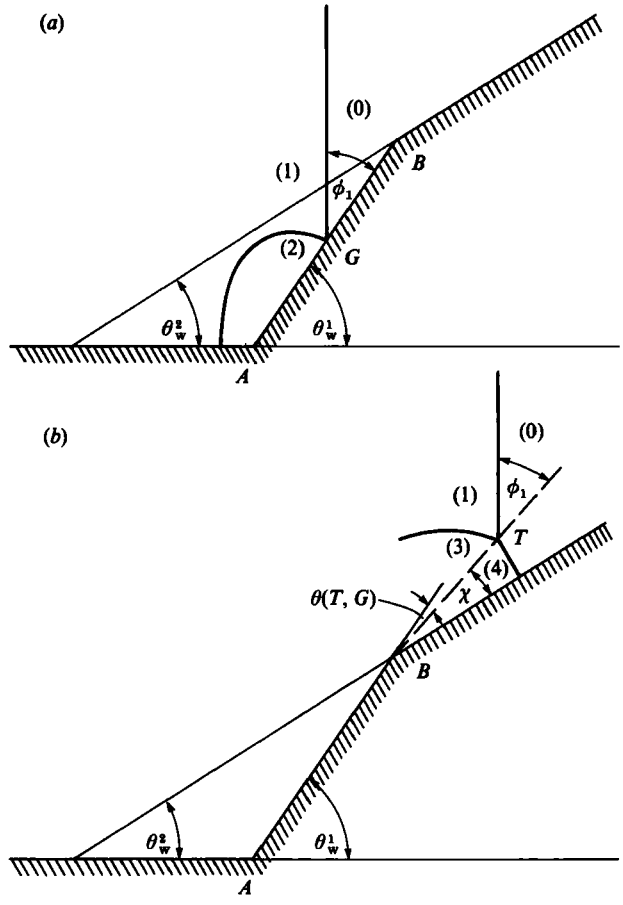

FIGURE 14. Schematic illustration of the shock-wave reflection process for region 4. (*a*) Regular reflection over the first wedge and (*b*) Mach reflection over the second wedge.

Region 4

In this region $\Delta\theta_w < 0$; $\theta_w^1 > \theta_w^{det}$, and $\theta_w^2 < \theta_w^{det}$, and the reflection process is shown schematically in figure 14. The incident shock reflects over the first wedge as a regular reflection (figure 14*a*) and upon encountering the second wedge there is a transition to a Mach reflection (figure 14*b*). The initial and final reflections can be made pseudo-stationary by attaching a frame of reference respectively to the reflection point G, or the triple point T.

The direction of the triple point T with respect to that of the reflection point G is given by

$$\theta(T, G) = -(-\Delta\theta_w - \chi). \tag{12}$$

A shock-polar solution for a typical reflection process in region 4 is shown in figure 15. The incident shock wave ($M_i = 2.5$) reflects over the first wedge ($\theta_w^1 = 60°$) as a regular reflection. However, since $\Delta\theta_w = -20°$, the second wedge, $\theta_w^2 = 40°$, cannot support a regular reflection, and a Mach reflection with $\chi = 5.29°$ is finally established over it.

The I^G and R^G shock polars represent the regular reflection over the first wedge,

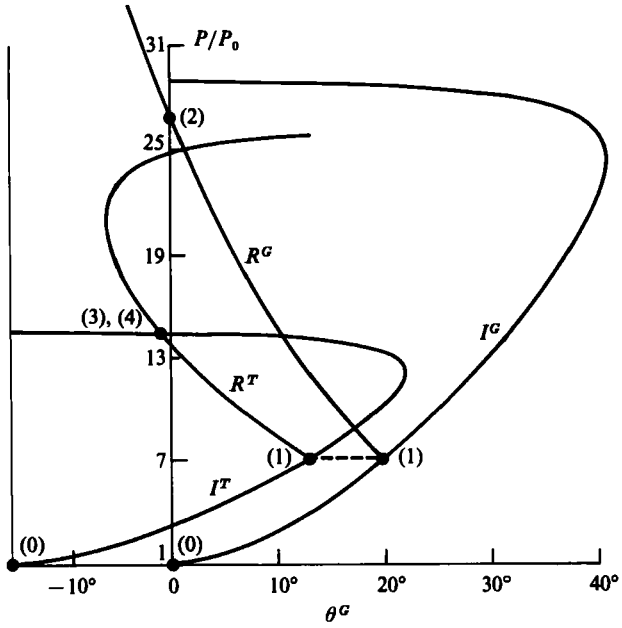

FIGURE 15. The shock-polar solution of the shock-wave reflection process in region 4. The polars are drawn accurately for an incident shock with Mach number $M_1 = 2.5$, and a double convex wedge with inclinations $\theta_w^1 = 60°$ and $\theta_w^2 = 40°$. The triple-point trajectory angle over the second wedge is $\chi = 5.29°$. I^G, R^G and I^T, R^T are the incident and reflected shock polars for pseudo-steady regular and Mach reflections respectively over the first and second wedges.

and the origin of the I^T and R^T shock polars, which represent the Mach reflection over the second wedge, are displaced by $(\Delta\theta_w + \chi)$, which is negative. The constant pressure P_1 behind the incident shock again bridges the two sets of polars. For this case the velocity of G is greater than that of T so that M_0^G is greater than M_0^T and the I^G polar is larger than I^T polar.

In general the pressure P_2 behind the reflected shock over the first wedge will be different from the pressure P_4 behind the Mach stem over the second wedge. A transition period is expected after the incident shock moves from the first to the second wedge with expansion or compression waves which will dissipate through the flow. It is not expected that these waves will persist as is predicted for the reflections in regions 1 and 2, and the Mach reflection over the second wedge will asymptotically approach that which would be produced if the incident shock had reflected from a single wedge with an inclination θ_w^2.

Region 5

In this region $\Delta\theta_w > 0; \theta_w^1 < \theta_w^{det}; \Delta\theta_w > \theta_w^{det}$, and $\theta_w^2 > \theta_w^{det}$, and the reflection process is shown schematically in figure 16. The incident shock reflects over the first wedge as a Mach reflection (figure 16*a*). The Mach stem of this reflection reflects over the second wedge as a regular reflection (figure 16*b*). The triple point T and the reflection point G_1 of the Mach and regular reflections interact at point Q on the second wedge surface to form a new regular reflection, with reflection point G_2 (figure 16*c*).

The reflections can be made pseudo-stationary by attaching frames of reference to the triple point T, or the points of reflection G_1 and G_2, as appropriate. The direction

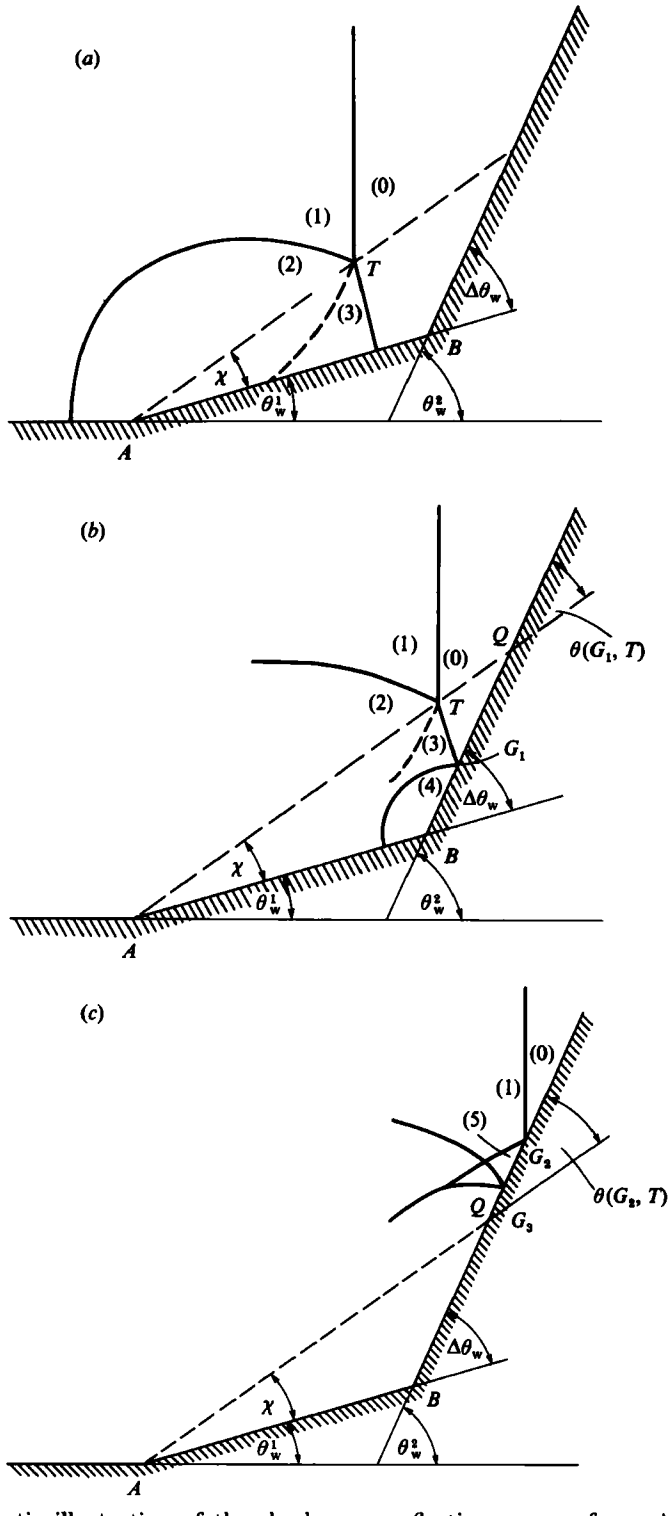

FIGURE 16. Schematic illustration of the shock-wave reflection process for region 5. Q is the intersection of the triple-point trajectory with the second wedge. (*a*) Mach reflection over the first wedge, (*b*) regular reflection over the second wedge and (*c*) the shock configurations after the incident shock has passed Q.

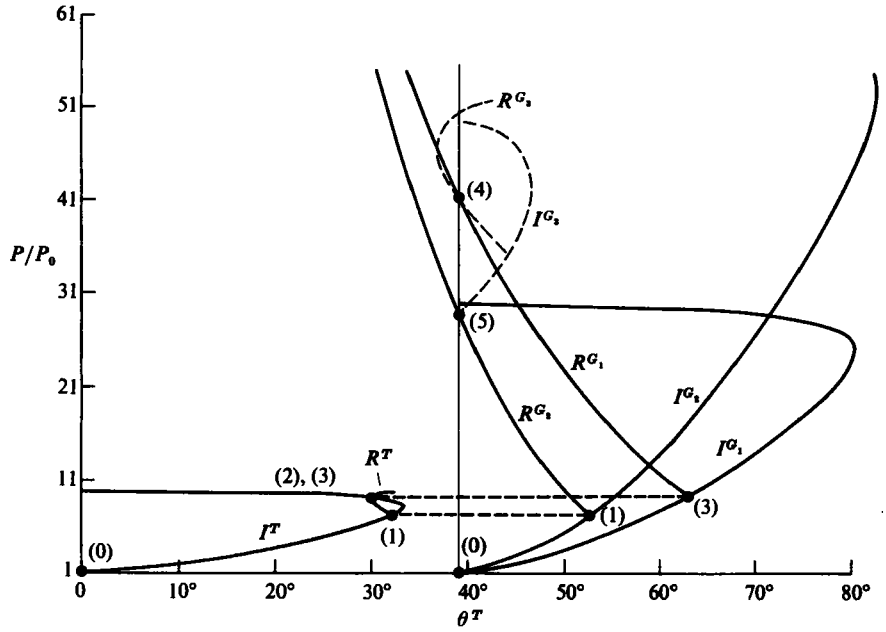

FIGURE 17. The shock-polar solution of the shock-wave reflection process in region 5. The polars are drawn acurately for an incident shock with Mach number $M_1 = 2.5$, and a double concave wedge with inclinations $\theta_w^1 = 15°$ and $\theta_w^2 = 70°$. The triple-point trajectory angle is $\chi = 15.72°$, and the Mach number of the Mach stem shock is $M_m = 2.8$. I^T and R^T are the incident and reflected shock polars for the pseudo-steady Mach reflection over the first wedge. I^{G_1}, R^{G_1} and I^{G_2}, R^{G_2} are the incident and reflected shock polars of the pseudo-steady regular reflections over the second wedge, before and after the intersection of the triple-point trajectory with the second wedge, respectively. The dashed I^{G_2}, R^{G_2} polars indicate the probable solution for the regular reflection which permits the pressure jump from state (4) to state (5) in figure 16. The polars are linked by the dashed lines representing the constant pressure in states (3) and (1) of figure 16.

of the reflection points G_1 and G_2 with respect to the direction of the triple point T are given by

$$\theta(G_1, T) = \Delta\theta_w - \chi, \tag{13}$$

and

$$\theta(G_2, T) = \Delta\theta_w - \chi. \tag{14}$$

A shock-polar solution for a typical reflection process in region 5 is shown in figure 17. The incident shock wave ($M_1 = 2.5$) reflects over the first wedge ($\theta_w^1 = 15°$) as a Mach reflection with $\chi = 15.72°$. The Mach number of the Mach stem of this reflection is $M_m = 2.8$. Since $\Delta\theta_w = 55°$, the Mach stem reflects over the second wedge as a regular reflection. Finally, the incident shock wave ($M_1 = 2.5$) encounters the second wedge ($\theta_w^2 = 70°$) from which it reflects regularly.

The I^T and R^T shock polars represent the Mach-reflection solution over the first wedge. Since the solutions of the two regular reflections over the second wedge are made from a frame of reference which is displaced by the angle $\theta(G_1, T)$ or $\theta(G_2, T)$ with respect to the original frame of reference, the origins of the I^{G_1}, R^{G_1} and the I^{G_2}, R^{G_2} shock polars, which represent the regular reflections over the second wedge are located at $\theta^T = \theta(G_1, T) = \theta(G_2, T) = \Delta\theta_w - \chi$. Since the pressures in states (1) and (3) are independent of the frame of reference from which the solution is carried out, the I^T, R^T and I^{G_1}, R^{G_1} shock polars are bridged by the constant P_3 line, and the

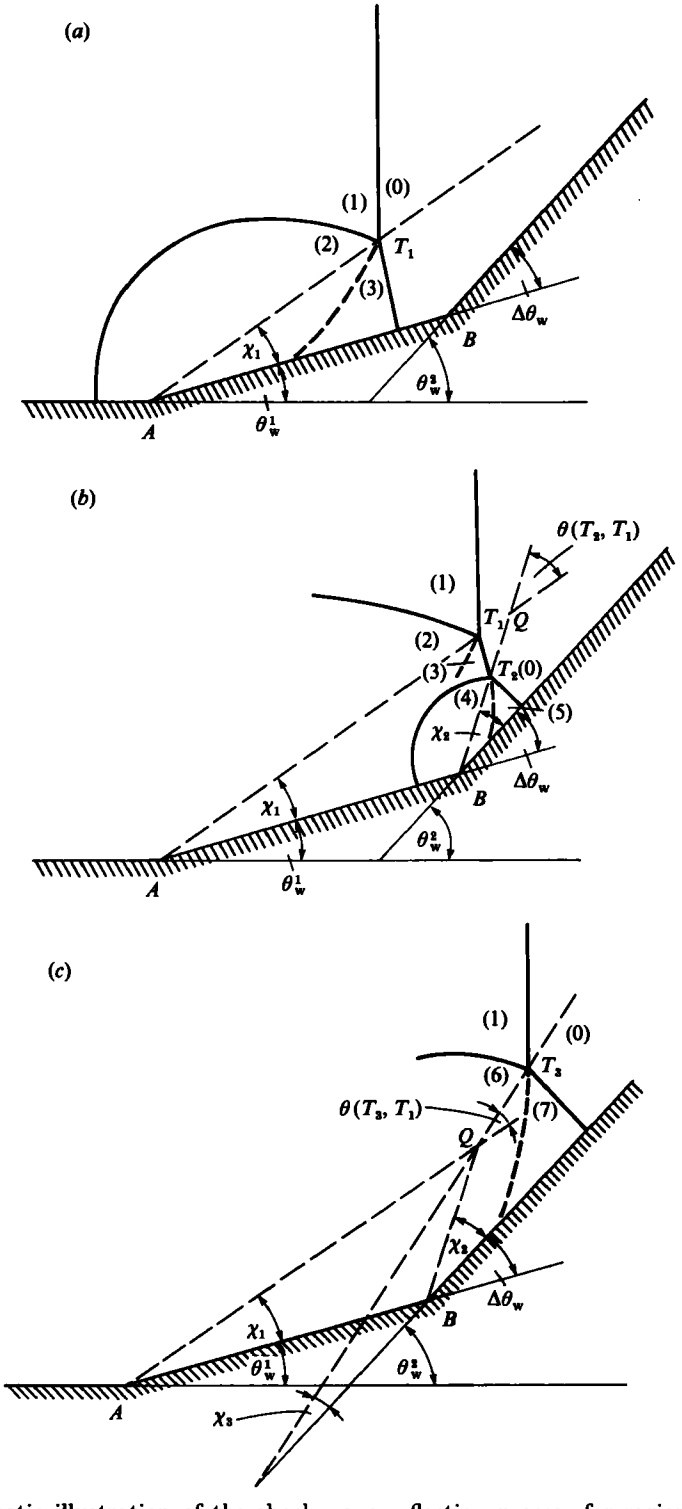

FIGURE 18. Schematic illustration of the shock-wave reflection process for region 6. (*a*) Mach reflection over the first wedge, (*b*) Mach reflection over the second wedge and (*c*) Mach reflection over the second wedge after the incident shock has passed Q, the point of intersection of the two triple-point trajectories.

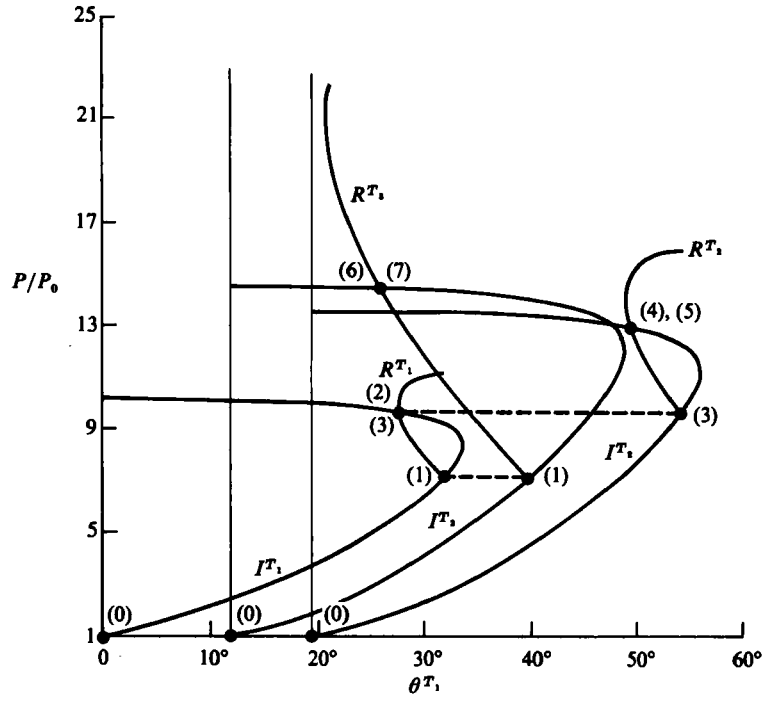

FIGURE 19. The shock-polar solution of the shock-wave reflection process in region 6. The polars are drawn accurately for an incident shock with Mach number $M_1 = 2.5$, and for a double concave wedge with inclinations $\theta_w^1 = 20°$ and $\theta_w^2 = 40°$. The Mach number of the Mach-stem shock over the first wedge is $M_m = 2.9$, and the triple-point trajectory angles are $\chi_1 = 12.85°$, $\chi_2 = 12.49°$ and $\chi_3 = 5.29°$. I^{T_1} and R^{T_1} are the incident and reflected shock polars of the pseudo-steady Mach reflection over the first wedge. I^{T_2}, R^{T_2} and I^{T_3}, R^{T_3} are the incident and reflected shock polars of the pseudo-steady Mach reflections over the second wedge, before and after the intersection of the triple-point trajectories, respectively. The polars are linked by the dashed lines representing the constant pressures in states (3) and (1) of figure 18.

I^T, R^T and I^{G_1}, R^{G_2} shock polars are bridged by the constant P_1 line, which are dashed in figure 17.

The shock polars in figure 17 indicate that the transition on the second wedge at point Q is associated with a sudden decrease in the pressure from P_4 behind G_1 to P_5 behind G_2. It will be shown subsequently that this sudden pressure drop is supported by an additional regular reflection, that of the reflected shock wave of the Mach reflection over the first wedge. This secondary regular reflection follows the main regular reflection over the second wedge. This additional regular reflection is drawn schematically in figure 16(*c*) with reflection point G_3. It is expected that the overall pressure jump across this additional regular reflection should be close to P_4/P_5. A dashed I^{G_3}, R^{G_3} polar combination representing this regular reflection is added to figure 17.

It will be shown subsequently that as this secondary regular reflection propagates up the wedge its reflected shock catches up with its incident shock to finally form a single shock wave normal to the wedge surface.

Region 6

In this region $\Delta\theta_w > 0; \theta_w^1 < \theta_w^{det}; \Delta\theta_w < \theta_w^{det}$, and $\theta_w^2 < \theta_w^{det}$, and the reflection process is shown schematically in figure 18. The incident shock reflects over the first

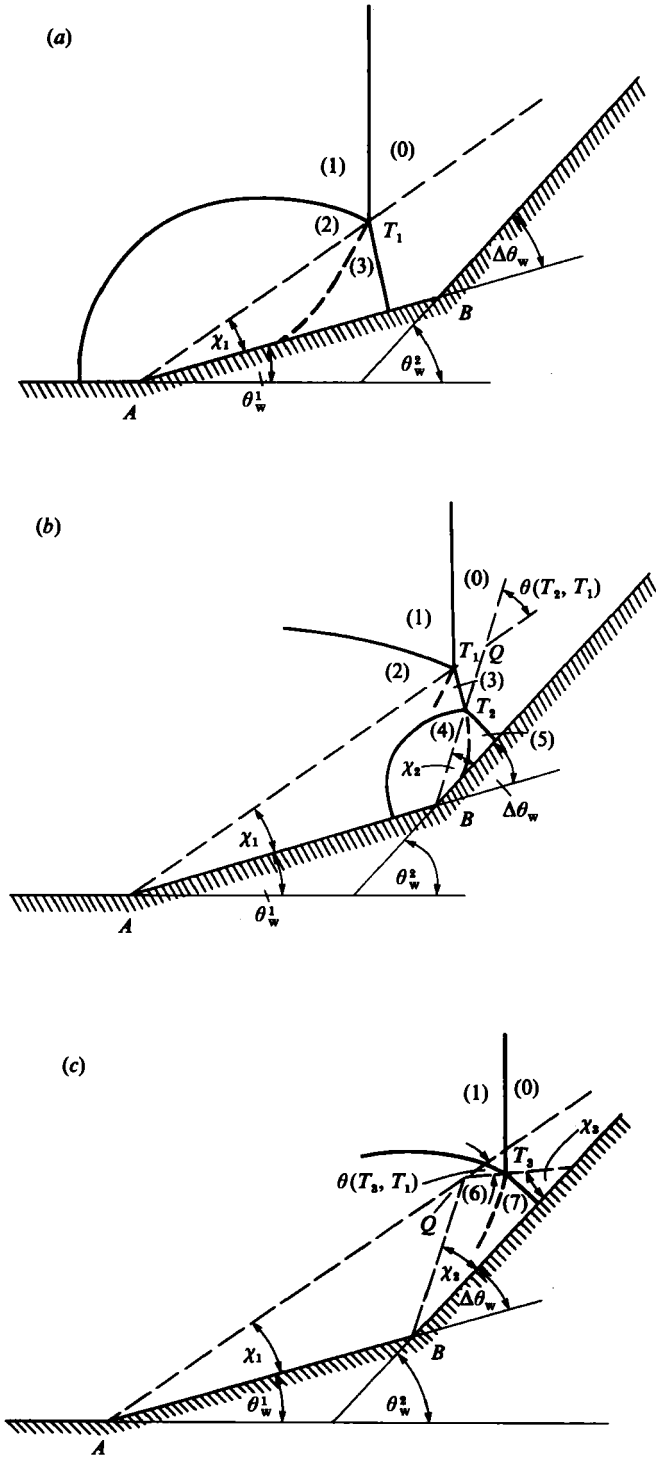

FIGURE 20(*a–c*). For caption see facing page.

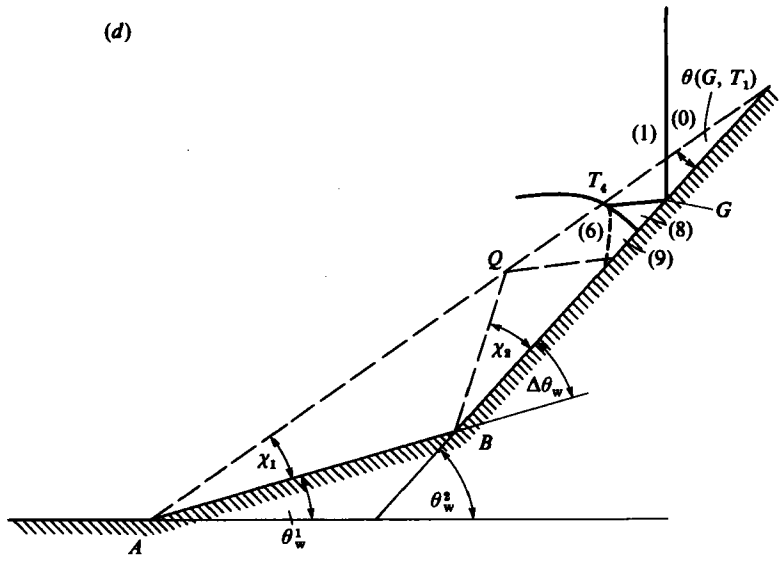

FIGURE 20. Schematic illustration of the shock-wave reflection process for region 7. (*a*) Mach reflection over the first wedge. (*b*) Mach reflection over the second wedge. Q is the intersection of the triple-point trajectories. (*c*) Inverse-Mach reflection over the second wedge after the incident shock has passed Q. (*d*) Regular reflection over the second wedge after the third triple point T_3 has reached the wedge surface.

wedge as a Mach reflection (figure 18*a*), and the Mach stem of this reflection reflects from the second wedge also as a Mach reflection (figure 18*b*). The triple points T_1 and T_2 of these two Mach reflections, intersect at Q to form a direct Mach reflection (figure 18*c*), for which the triple point moves away from the second-wedge surface. Therefore, the Mach reflection is maintained. It is assumed that these three Mach reflections can be made pseudo-stationary by attaching frames of reference to their appropriate triple points. The directions of T_2 and T_3 with respect to the direction of T_1 are given by

$$\theta(T_2, T_1) = \Delta\theta_w + \chi_2 - \chi_1, \tag{15}$$

and

$$\theta(T_3, T_1) = \Delta\theta_w + \chi_3 - \chi_1. \tag{16}$$

A shock-polar solution for a typical reflection process in region 6 is shown in figure 19. The incident shock wave ($M_i = 2.5$) reflects over the first wedge ($\theta_w^1 = 20°$) as a Mach reflection with $\chi_1 = 12.85°$. The Mach number of the Mach stem of this reflection is $M_m = 2.9$. Since $\Delta\theta_w = 20°$, the Mach stem reflects over the second wedge as a Mach reflection with $\chi_2 = 12.42°$. Finally, after the interaction between the two triple points, at Q, the incident shock wave ($M_i = 2.5$) forms a Mach reflection over the second wedge ($\theta_w^2 = 40°$) with $\chi_3 = 5.29°$.

The I^{T_1} and R^{T_1} polars represent the Mach reflection over the first wedge and the origins of the I^{T_2}, R^{T_2} and I^{T_3}, R^{T_3} polars, for the second and third Mach reflections are located at $\theta^{T_1} = \theta(T_2, T_1)$ and $\theta^{T_1} = \theta(T_3, T_1)$ respectively. Since the pressures in states (1) and (3) are independent of the frame of reference, the I^{T_1}, R^{T_1} and I^{T_2}, R^{T_2} polars are bridged by the constant P_3 line, and the I^{T_1}, R^{T_1} and I^{T_3}, R^{T_3} polars are bridged by the constant P_1 line, which are dashed in figure 19.

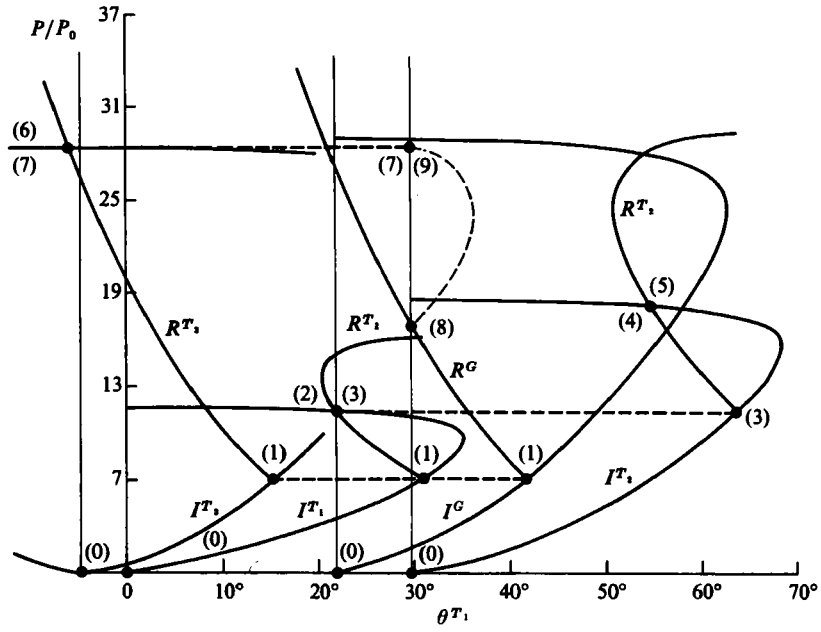

FIGURE 21. The shock-polar solution of the shock-wave reflection process in region 7. The polars are drawn accurately for an incident shock with Mach numbers $M_i = 2.5$, and a concave double wedge with inclinations $\theta_w^1 = 30°$, and $\theta_w^2 = 60°$. The Mach number of the Mach-stem shock over the first wedge is $M_m = 3.15$, and the triple-point trajectory angles are $\chi_1 = 8.27$, $\chi_2 = 8.09°$ and $\chi_3 = -1.12°$. I^{T_1} and R^{T_1} are the shock polars for the pseudo-stationary Mach reflection over the first wedge. I^{T_2}, R^{T_2} and I^{T_3}, R^{T_3} are the shock polars for the pseudo-steady Mach reflections over the second wedge, before (direct-Mach) and after (inverse-Mach) the intersection of the triple-point trajectories, respectively. I^G and R^G are the shock polars for the ultimate pseudo-steady regular reflection over the second wedge. The dashed polar represents the probable solution for the normal shock which permits the pressure jump from state (8) to (9) in figure 20(*d*). The polars are linked by the dashed lines representing the constant pressures in states (1), (3) and (7) of figure 20.

The changes of pressure along the wedge from P_5 to P_7 at the time when the triple points T_1 and T_2 interact at Q and form the third Mach reflection with a different Mach stem, will result in the generation of compression or expansion waves but these are expected to dissipate in the flow and not to persist as in regions 1 and 2.

Region 7

In this region $\Delta\theta_w > 0; \theta_w^1 < \theta_w^{det}; \Delta\theta_w < \theta_w^{det}$, and $\theta_w^2 > \theta_w^{det}$, and the reflection process is shown schematically in figure 20. The incident shock reflects over the first wedge as a Mach reflection (figure 20*a*), and the Mach stem reflects from the second wedge also as a Mach reflection (figure 20*b*). The triple points T_1 and T_2 intersect at Q to form a third Mach reflection (figure 20*c*). Unlike the reflection in region 6, the new triple point T_3 moves towards the second wedge surface, i.e. the Mach reflection is an inverse-Mach reflection (Takayama & Ben-Dor 1985). Upon colliding with the wedge surface, the inverse-Mach reflection transitions to a regular reflection, which continues to propagate up the wedge (figure 20*d*).

It is assumed that the three Mach reflections and the final regular reflection can be made pseudo-stationary by attaching a frame of reference to the appropriate triple

points T_1, T_2 or T_3, or the reflection point G. The directions of T_2, T_3 and G with respect to the direction of T_1 are given by

$$\theta(T_2, T_1) = \Delta\theta_w + \chi_2 - \chi_1; \tag{17}$$

$$\theta(T_3, T_1) = -(-\Delta\theta_w + \chi_3 + \chi_1), \tag{18}$$

$$\theta(G, T_1) = \Delta\theta_w - \chi_1. \tag{19}$$

A shock-polar solution for a typical reflection process in region 7 is shown in figure 21. The incident shock ($M_i = 2.5$) reflects over the first wedge ($\theta_w^1 = 30°$) as a Mach reflection with $\chi_1 = 8.27°$. Since $\Delta\theta_w = 30°$, the Mach stem ($M_m = 3.15$) reflects over the second wedge as a Mach reflection with $\chi_2 = 8.09°$. Eventually, the two triple points intersect at Q and the incident shock ($M_i = 2.5$) propagates over the secondary wedge ($\theta_w^2 = 60°$) from which it reflects regularly.

The I^{T_1}, R^{T_1} shock polars represent the Mach-reflection solution over the first wedge, and the origins of the I^{T_2}, R^{T_2} and I^{T_3}, R^{T_3} shock polars, which represent the second and the third Mach reflections are located at $\theta^{T_1} = \theta(T_2, T_1)$ and $\theta^{T_1} = \theta(T_3, T_1)$, respectively. Since the pressures in states (1) and (3) are independent of the frames of reference, the I^{T_1}, R^{T_1} and I^{T_2}, R^{T_2} shock polars are bridged by the constant P_3 line, and the I^{T_1}, R^{T_1} and I^{T_3}, R^{T_3} shock polars are bridged by the constant P_1 line. Since the third Mach reflection is an inverse-Mach reflection, its polar solution (states 6 and 7) takes place on the left part of the I^{T_3} polar (for details see Takayama & Ben-Dor 1985). For clarity, parts of the I^{T_3} polar have been omitted from figure 21.

The origin for the final regular reflection is at $\theta^{T_1} = \theta(G, T_1)$. The I^G, R^G polar combination which represents the regular reflection is also bridged to the I^{T_1}, R^{T_1} polars through the constant P_1 line.

The shock polars in figure 21 suggest that a sudden pressure drop will occur from P_7 just before the termination of the inverse-Mach reflection, to P_8, just after the formation of the regular reflection. It was found experimentally that, unlike the case, in region 5, where the sudden pressure drop is supported by a secondary regular reflection (figure 16*c*), here it is supported by a normal shock wave which follows the regular reflection. This normal shock wave is shown in figure 20(*d*). It is expected that the pressure jump across this normal shock wave should be close to P_6/P_8. A dashed polar representing this normal shock wave is added to figure 21. In figure 20 the state behind the normal shock wave is labelled as state (9), and hence the pressure jump across it is P_9/P_8, however states (9) and (6) and states (6) and (7) are separated by slipstreams and hence $P_7 = P_9$.

3. Experimental investigations

The reflection of plane shock waves from concave and convex double wedges was studied experimentally using the 7.6 cm × 25.4 cm shock tube of the Department of Physics at the University of Victoria, Canada, and the 7.6 cm × 12.7 cm shock tube of the Institute of High Speed Mechanics, Tohoku University, Japan. The objectives of the experimental studies were to establish the conditions for transition from regular to Mach reflection or Mach to regular reflection (RR $\rightleftarrows$ MR) for concave and convex double wedges; to verify the existence of the seven reflection processes predicted in the foregoing analysis, and to verify the predictions of the shock-polar analysis concerning the wave configurations following the major reflections. These objectives were achieved using various high-speed photographic techniques such as contact shadowgraphs, multi-frame schlieren and holographic interferometry.

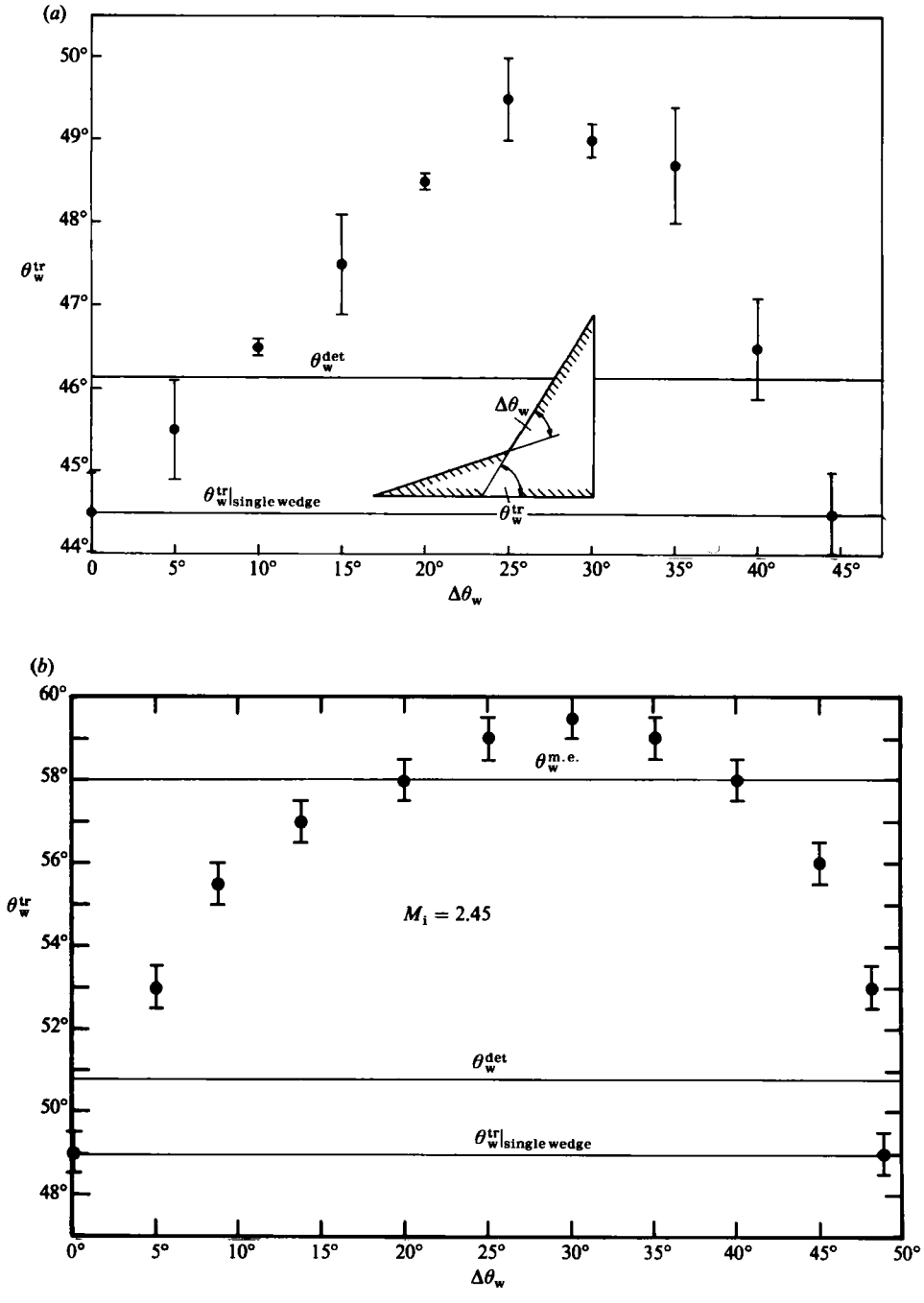

FIGURE 22. The angle of the second wedge at which transition from regular to Mach reflection was observed, θ_w^{tr}, as a function of $\Delta\theta_w$ for a concave double wedge: (*a*) weak shock wave $M_i = 1.29 \pm 0.01$. (*b*) strong shock wave $M_i = 2.45 \pm 0.01$.

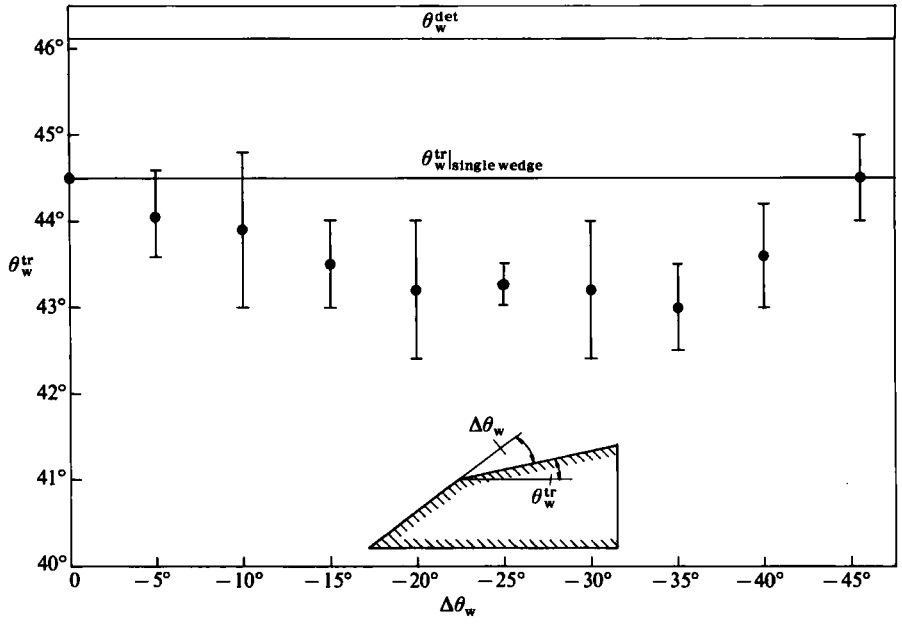

FIGURE 23. The angle of the second wedge at which transition from regular to Mach reflection was observed, θ_w^{tr}, as a function of $\Delta\theta_w$ for a convex double wedge and $M_1 = 1.29 \pm 0.01$.

4. RR $\rightleftarrows$ MR transition wedge angle

Using nominal incident-shock Mach numbers of 1.3 and 2.45, the angle of the second wedge at which RR $\rightleftarrows$ MR occurred, was determined. Experiments were conducted using double wedges, similar to those shown in figure 4. Depending upon the final reflection which was observed over the second surface, the second wedge angle, θ_w^2, was increased or decreased by tilting the double wedge until the reflection over the second surface changed from MR to RR or from RR to MR.

The lowest value of θ_w^2 for which RR was observed, and the highest value of θ_w^2 for which MR was observed were averaged to give an estimate of θ_w^{tr} and the associated uncertainty.

In the 'weak'-shock experiments there were small variations in the incident-shock Mach number from experiment to experiment but all were in the range $1.28 \leqslant M_1 \leqslant 1.30$. The theoretical detachment transition wedge angle for this range of Mach numbers is $45.899° \leqslant \theta_w^{det} \leqslant 46.347°$. The wedge angles, θ_w^{tr}, at which transition was observed on the second wedge are plotted as a function of $\Delta\theta_w$ for a concave double wedge in figure 22(*a*). At $\Delta\theta_w = 0$, i.e. the case of a straight single wedge, the measured value of θ_w^{tr} is about 1.5° smaller than the theoretical detachment value. This observation is in accordance with experimental results of many other investigators and is probably due to boundary-layer effects. The same value is obtained at $\Delta\theta_w = 44.5°$ which again represents the case of a single straight wedge, since for this case $\theta_w^1 = 0$.

For the specific incident-shock Mach mumber of these experiments, $M_1 = 1.29 \pm 0.01$, the transition angle, θ_w^{tr} reaches a maximum of approximately 49.5° for a double wedge with $\Delta\theta_w = 25°$. It is interesting to note that in the range $0 \leqslant \Delta\theta_w \leqslant 25°$ there appears to be a linear relationship between θ_w^{tr} and $\Delta\theta_w$. The

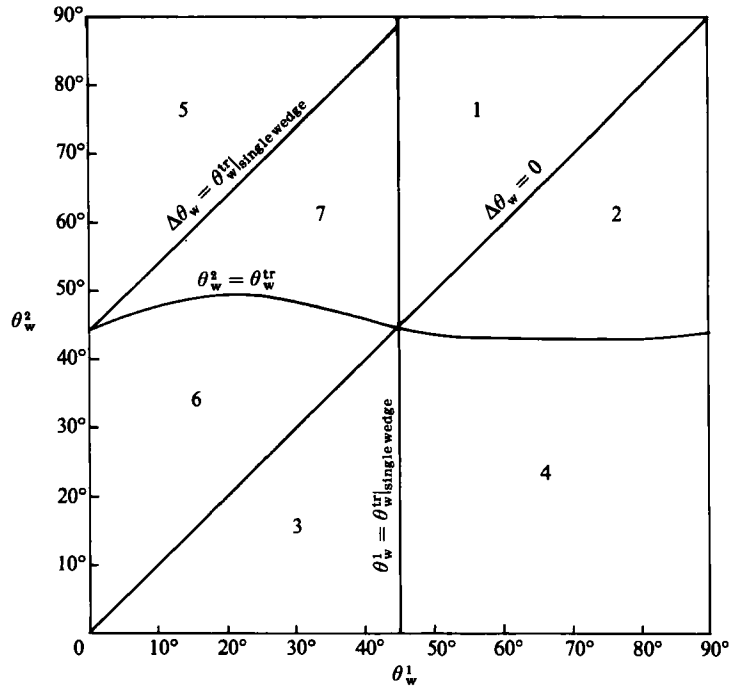

FIGURE 24. Actual regions and transition boundaries of the seven different reflection processes for an incident shock wave with $M_1 = 1.29 \pm 0.01$ over a double wedge.

overall relationship between θ_w^{tr} and $\Delta\theta_w$ for a concave double wedge may be compared with that between θ_w^{tr} and R, the radius of curvature of a concave cylindrical wedge for which the transition angle is also greater than that over a single plane wedge (Ben-Dor *et al.* 1980).

The measured transition wedge angles for a strong shock wave ($M_1 > M_1^*$) over a concave double wedge are shown in figure 22(*b*). For these cases $M_1 = 2.45 \pm 0.01$. The transition wedge angles for $\Delta\theta_w = 0$ and $\Delta\theta_w = 49°$ which correspond to a single straight wedge are about 1.7° below the value predicted by the 'detachment' criterion ($\theta_w^{det} = 50.77°$). This persistence is probably due to boundary-layer effects. As $\Delta\theta_w$ increases the transition wedge angle becomes higher until it reaches a maximum of $\theta_w^{tr} = 59.5°$ at $\Delta\theta_w = 30°$. This value of θ_w^{tr} is greater than the 'mechanical-equilibrium' transition wedge angle for this Mach number ($\theta_w^{m.e.} = 58°$). For $\Delta\theta_w > 30°$ the transition wedge angle decreases until it reaches the value appropriate to a single wedge at $\Delta\theta_w = 49°$. It should be noted that for this case of a strong incident shock wave the transition wedge angles lie between the 'detachment' and the 'mechanical-equilibrium' transition wedge angles. To the best of our knowledge this is the first time that the RR $\rightleftarrows$ MR transition has been observed in this range of wedge angle.

Figure 23 shows the observed transition wedge angles, θ_w^{tr}, as a function of $\Delta\theta_w$ for a convex double wedge and an incident shock Mach number of 1.29 ± 0.01. In this case $\Delta\theta_w = 0$ corresponds to the single wedge case with $\theta_w^{tr} = 44.5°$. For decreasing values of $\Delta\theta_w$ the transition angle decreased to a minimum of about 43.25° for $\Delta\theta_w$ in the range from $-20°$ to $-35°$, and then returned to 44.5° at $\Delta\theta_w = -45.5°$, which also corresponds to a single straight wedge. The variation of θ_w^{tr} with $\Delta\theta_w$ over a convex double wedge may be compared with the variation of θ_w^{tr} with the radius of

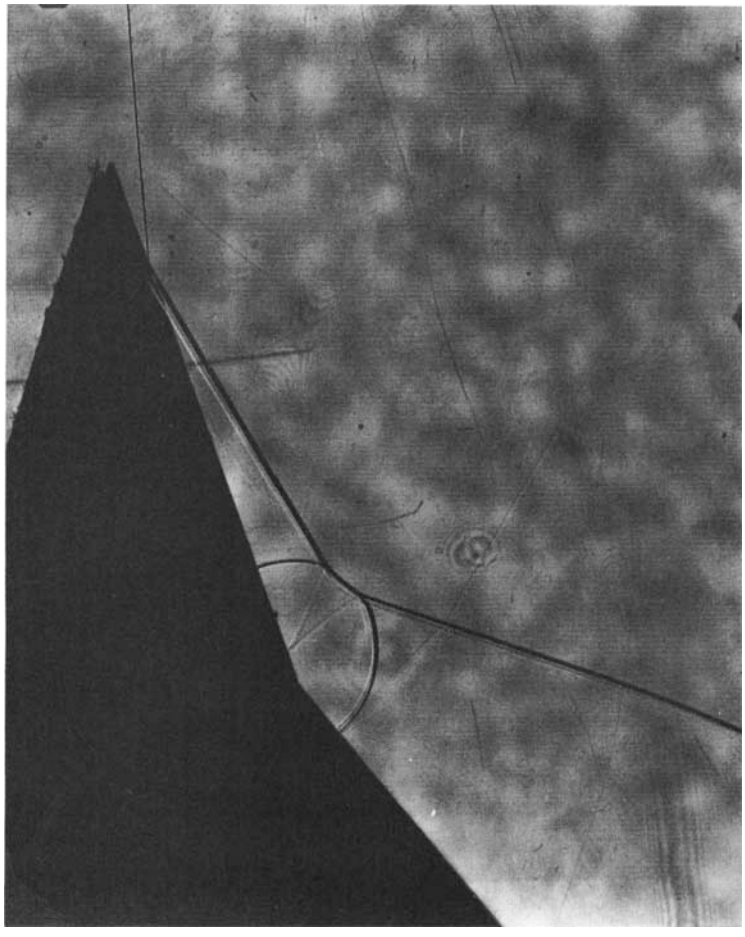

FIGURE 25. Shadowgraph illustrating the reflection on the second wedge, following a regular reflection on the first wedge for a double wedge in region 1. $\theta_w^1 = 55°$ and $\theta_w^2 = 75°$.

curvature of a convex cylinder for which the observed transition angle is also less than the theoretical detachment angle, θ_w^{det}, and the observed transition angle on a straight wedge (Ben-Dor *et al.* 1980).

The observed transition wedge angles presented in figures 22(*a*) and 23 were used to modify the boundaries between regions 6 and 7, and 2 and 4 in figure 5, and the modification is presented as figure 24.

5. Experimental verification of the reflection processes

Experiments were carried out using combinations of wedge angles representative of each of the seven regions defined by figure 24, using a nominal incident-shock Mach number of 1.3. The shock reflections were observed using two photographic methods: multiple double-pass laser schlieren at a framing rate of approximately 20000 p.p.s., and single-frame contact shadowgraphy. In each case the exposure time per frame was approximately 50 ns. The shadowgraphs produced very high quality distortion-less pictures, but they did not reveal details of the density variations behind the

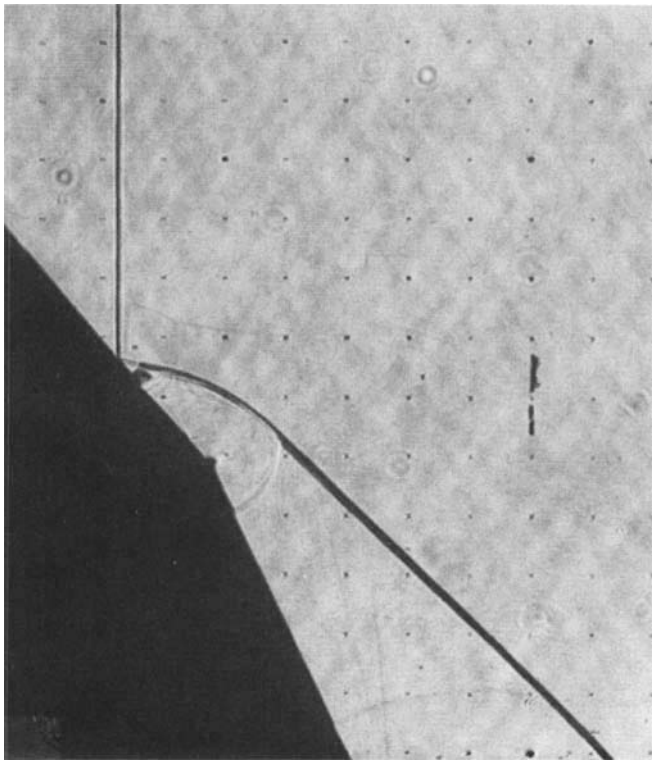

FIGURE 26. Schlieren photograph illustrating the reflection on the second wedge following a regular reflection on the first wedge for a double wedge in region 2. $\theta_w^1 = 65°$ and $\theta_w^2 = 50°$. Details of the wave structure behind the second regular reflection can be seen.

shocks to the same degree as the schlieren photographs. The double-pass schileren system has been described by Dewey & Walker (1975). The normally reflecting mirror in this system has a 1 cm grid of small holes through which smoke can be injected as a flow tracer. Smoke was not used in the experiments discussed here, but the holes served as a grid of fiducial markers.

Region 1

The final reflection process in this region is shown in figure 25 for $\theta_w^1 = 55°$ and $\theta_w^2 = 75°$. The regular reflection over the first wedge encounters the second compressive wedge, and the flow is compressed. The compression waves generated at the corner merge into two circular shock waves. One propagates upstream and follows the reflection point of the regular reflection and the other propagates downstream. They are both perpendicular to the wedge surface. These two circular shock waves interact with the reflected shock wave of the second and first regular reflections to form two triple points. The slipstreams of these triple points coincide at a point on the wedge. This point propagates upstream along the second wedge surface. The information about the change in the slope of the surface is probably bounded by these two shock waves.

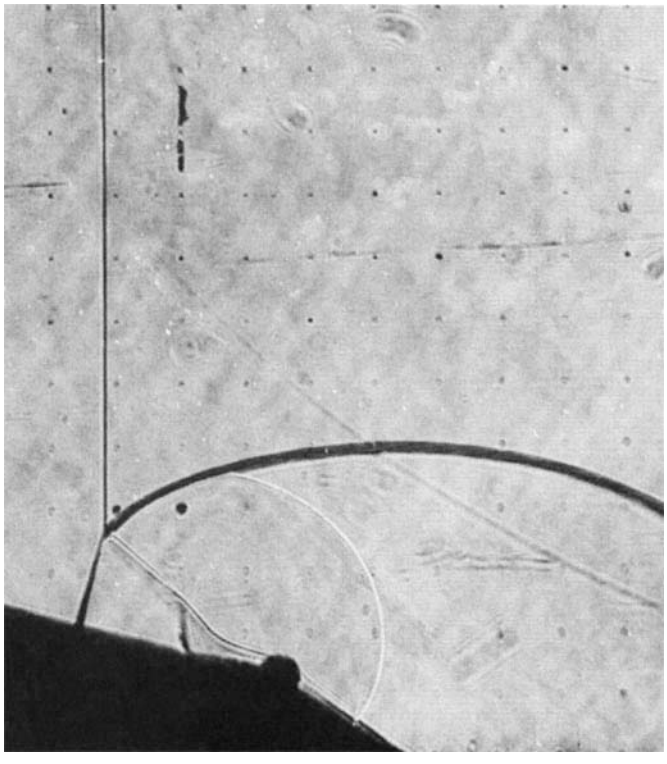

FIGURE 27. Schlieren photograph illustrating the Mach reflection on the second wedge following a Mach reflection on the first wedge for a double wedge in region 3. $\theta_w^1 = 35°$ and $\theta_w^2 = 15°$. The effects of the expansion wave generated when the Mach reflection moves from the first to the second wedge can be seen.

Region 2

The final reflection process in this region is shown as a schlieren photograph in figure 26 for $\theta_w^1 = 65°$ and $\theta_w^2 = 50°$. The regular reflection over the first wedge encountered an expansive corner which generated expansion waves, which can be seen in the figure, one propagating downstream just behind the reflection point, and the other propagating upstream along the first wedge. The combination of θ_w^1 and θ_w^2 in this experiment lies in region $2a$ of figure 11 and it is expected that the pressure in the small region behind the reflected shock and the rarefaction is at a higher pressure than behind the reflected shock on the first wedge.

Region 3

The schlieren photograph of the unsteady wave system, generated when the first Mach stem encounters the sudden change in the slope of the surface is shown in figure 27 for $\theta_w^1 = 35°$ and $\theta_w^2 = 15°$. A rarefaction wave is seen to be travelling backwards carrying the information about the sudden change in the model geometry. This corner signal causes the readjustment of the wave angles of the second Mach reflection needed to negotiate the new slope of the second wedge. As the rarefaction produced at the corner advanced up the first Mach stem it produced a weaker shock over the second surface. The contact surface separating the gases behind the stronger and

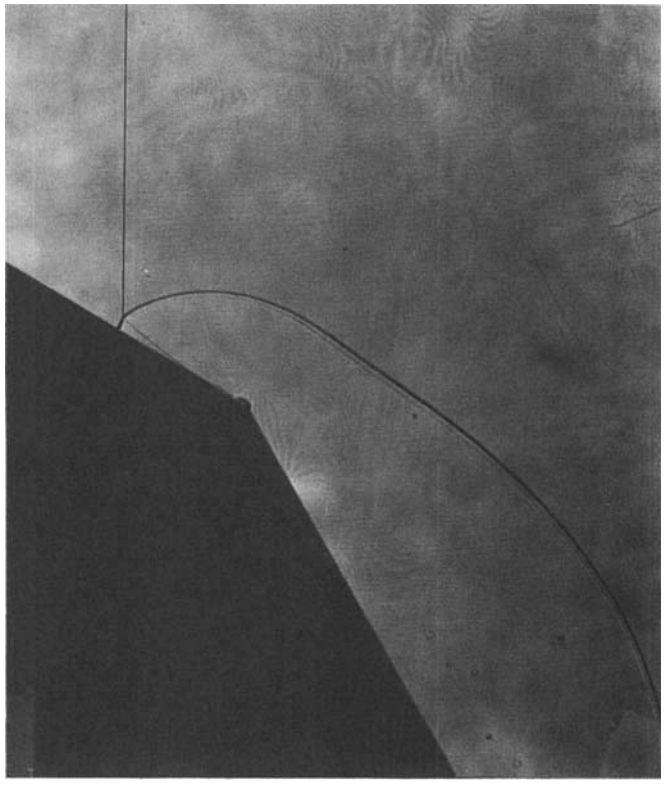

FIGURE 28. Shadowgraph of the Mach reflection on the second wedge, following a regular reflection on the first wedge for a double wedge in region 4: $\theta_w^1 = 60°$ and $\theta_w^2 = 30°$.

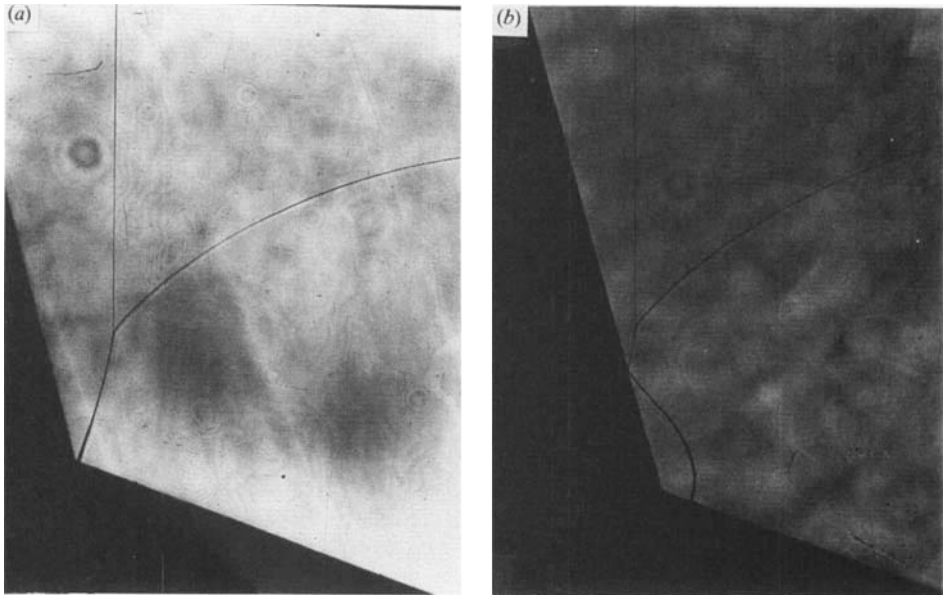

FIGURE 29(a, b). For caption see facing page.

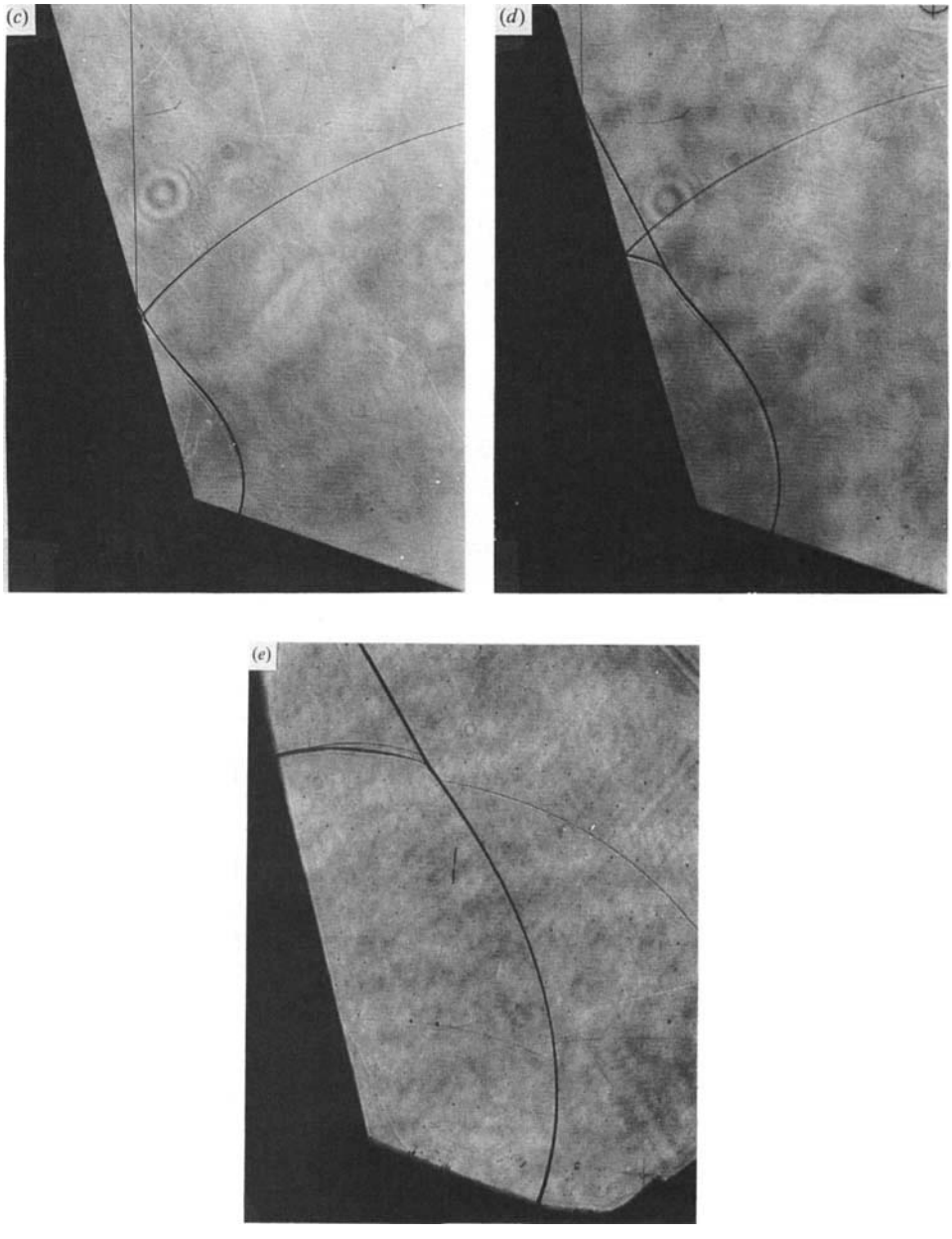

FIGURE 29. Shadowgraphs illustrating the reflection process over a double wedge in region 5. $\theta_w^1 = 20°$ and $\theta_w^2 = 75°$. (*a*) Mach reflection over the first surface. (*b*) The reflection of the Mach stem as a regular reflection from the second surface. (*c*) The wave structure immediately after the interaction between the triple point of the Mach reflection and the reflection point of the regular reflection. (*d*) The final regular reflection over the second surface followed by a regular reflection of the reflected shock of the Mach reflection which was terminated earlier. (*e*) The degeneration of the secondary regular reflection into a normal shock wave.

weaker shocks, until the rarefaction reached the triple point, can be clearly seen in figure 27.

Region 4

The final reflection process in this region is shown in figure 28 for $\theta_w^1 = 60°$ and $\theta_w^2 = 30°$. The regular reflection over the first surface encounters the sudden change in the slope and forms a Mach reflection over the second surface. The rarefaction wave generated at the corner, carries the information about the sudden change in the wedge geometry and causes the reflection to adjust its wave angles to negotiate the new slope of the second wedge.

Region 5

The reflection process in this region is shown in figure 29(*a–e*) for $\theta_w^1 = 20°$ and $\theta_w^2 = 75°$. The Mach reflection over the first wedge is shown in figure 29*a*. Its collision with the second wedge results in a regular reflection (figure 29*b*). The triple point of the Mach reflection over the first wedge and the reflection point of the regular reflection of the Mach stem over the second wedge interact on the second wedge. Figure 29(*c*) was recorded shortly after this interaction. The reflected shock wave of the Mach reflection now lags behind the incident shock wave. A clearer configuration of the wave system at a later time is shown in figure 29(*d*). The incident shock wave reflects from the second surface regularly. The reflected shock of the original Mach reflection reflects regularly from the second surface, and follows the major regular reflection. As this secondary regular reflection propagates along the wedge the wave angles of the incident and reflected shocks change until they merge together and form a single shock normal to the reflection surface, as shown in figure 29(*e*).

Region 6

The reflection process in this region is shown in figure 30(*a–c*) for $\theta_w^1 = 15°$ and $\theta_w^2 = 35°$. The Mach stem of the Mach reflection over the first wedge reflects from the second wedge also as a Mach reflection (figure 30*b*). The two triple points later interact (figure 30*b*) resulting in a direct Mach reflection of the incident shock wave over the second wedge. A second triple point is formed at the intersection of the two reflected shocks, as shown in figure 30(*c*), but the slipstream from this triple point is not visible in the shadowgraph.

Region 7

The reflection process in this region is shown in figure 31(*a*, *b*) for $\theta_w^1 = 25°$ and $\theta_w^2 = 60°$. The Mach stem of the Mach reflection over the first wedge reflects over the second wedge as a Mach reflection (figure 31*a*). The two triple points interact to give an inverse-Mach reflection (Takayama & Ben-Dor 1986), i.e. its triple point propagates towards the second wedge surface. When it meets the second surface the inverse-Mach reflection terminates and a regular reflection is formed, as shown in figure 31(*b*). The reflection is followed by a shock wave which is perpendicular to the second wedge surface, and which meets the reflected shock at a triple point. Another triple point is generated by the reflected shock waves of the two Mach reflections. The slipstreams of the two triple points can be seen in the shadowgraph of figure 31(*b*).

The final wave configuration shown in figure 31(*b*) is similar to the one finally obtained through the reflection process of region 5. However, the normal shock wave

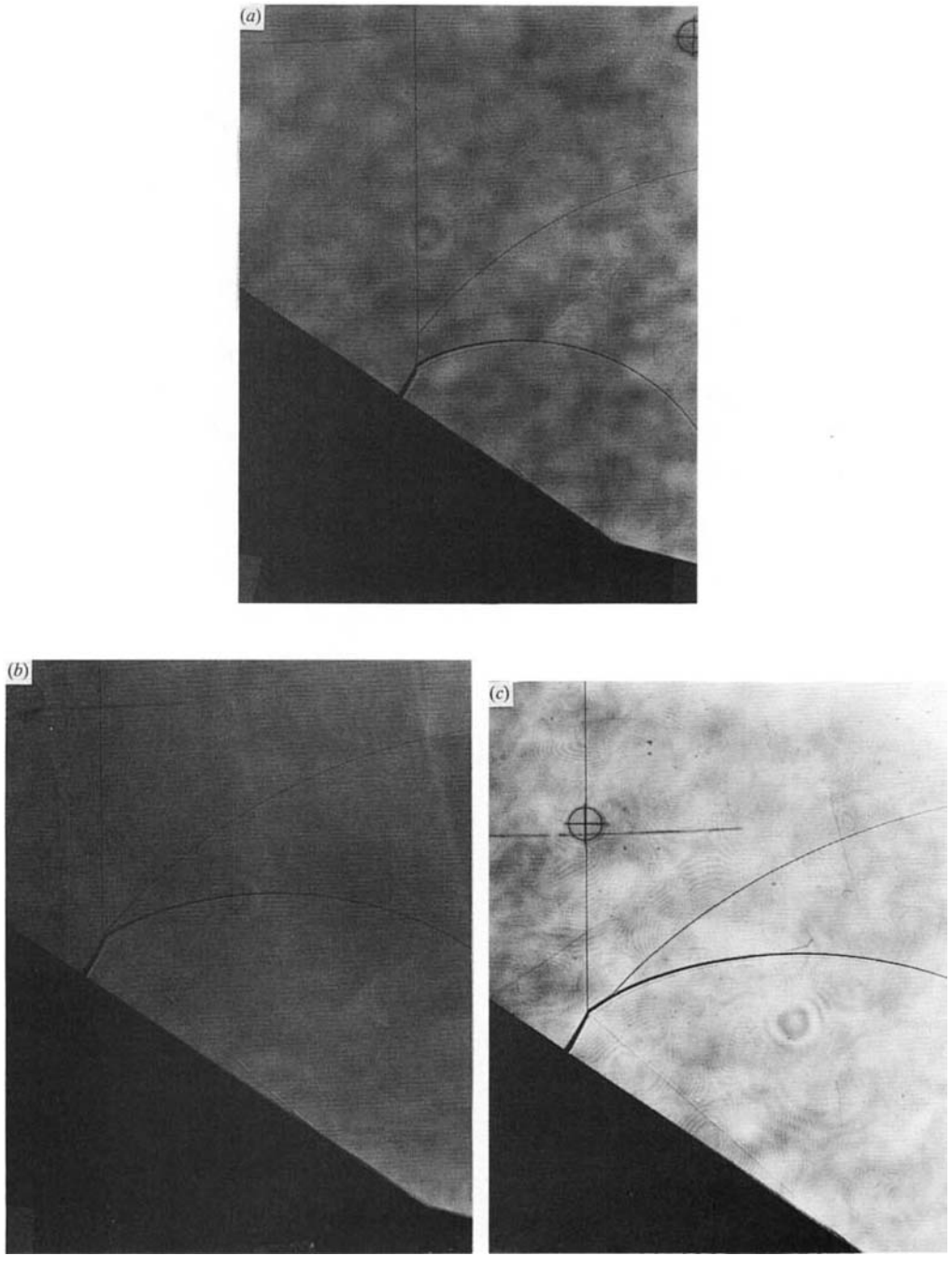

FIGURE 30. Shadowgraphs illustrating the reflection process over a double wedge in region 6. $\theta_w^1 = 15°$ and $\theta_w^2 = 35°$. (*a*) The reflection of the Mach stem from the first wedge over the second surface as a Mach reflection. (*b*) The interaction of the two triple points. (*c*) The final Mach reflection over the second wedge surface.

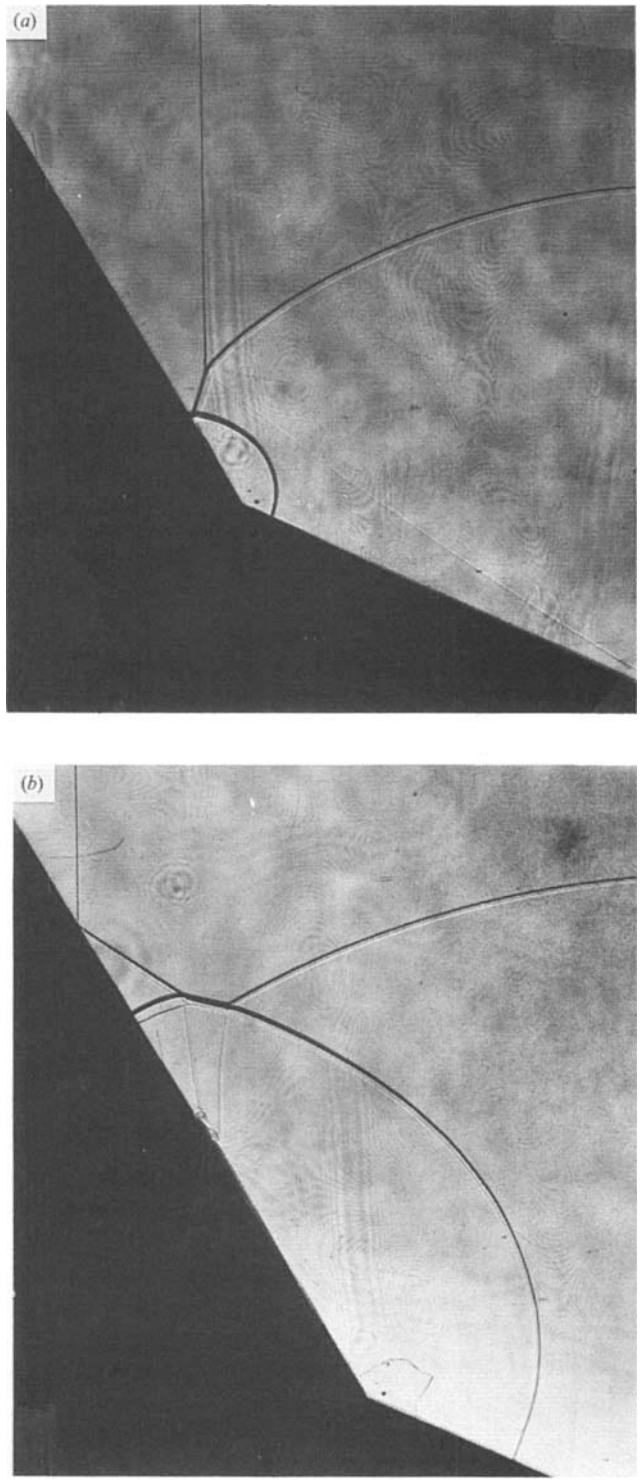

FIGURE 31. Shadowgraphs illustrating the reflection process over a double wedge in region 7. $\theta_w^1 = 25°$ and $\theta_w^2 = 60°$. (*a*) The reflection of the Mach stem from the first wedge over the second surface as a Mach reflection. (*b*) The final reflection over the second surface followed by a normal shock wave.

	θ_{w_1}	θ_{w_2}	$\Delta\theta_w$	First surface	Second surface	Region
Convex	> det	> det	—	Regular	Regular	2
	< det	< det	—	Mach	Mach	3
	> det	< det	—	Regular	Mach	4
Concave	> det	> det	—	Regular	Regular	1
	< det	> det	> det	Mach	Regular → Regular	5
	< det	< det	< det	Mach	Mach → Mach	6
	< det	> det	< det	Mach	Mach → Regular	7

TABLE 1. A summary of the seven different reflection processes which can occur over convex and concave double wedges depending on the magnitude of the wedge angles θ_w^1, θ_w^2 and $\Delta\theta_w$ compared to the detachment wedge angle θ_w^{det} (referred to simply as 'det' above). The numbers in the final column refer to the regions in the θ_w^1, θ_w^2 plane of figure 5.

in region 6 was established at the moment the inverse-Mach reflection terminated at the wedge surface, while in region 5 the initial reflection is a regular reflection which degenerates into a normal shock wave.

6. Conclusions

The reflection processes of a plane shock wave over a concave or convex double wedge, have been analysed using the basic concepts of the reflection of a plane shock wave over a single wedge. It was found that there are seven different reflection processes, which are summarized in table 1.

To simplify the analysis of the shock reflection processes a number of assumptions were made, namely, that transition between regular and Mach reflection would take place according to the theoretical 'detachment' criterion; that all Mach stems would be straight, and that the same 'detachment' transition angle could be used for both the incident and Mach stem shock waves. It is known that transition between regular and Mach reflection over a wedge does not occur at the angle predicted by theory; that for most shock strengths the Mach stem shock is curved, and that there will be a slight difference in the transition angle for the incident and Mach stem shock waves. Nevertheless we believe that the shock reflection processes described here are qualitatively correct.

For each of the seven reflection processes a shock-polar analysis was carried out. These analyses have provided information about the detailed wave structures following the main reflections along the wedge surfaces, and have made it possible to identify the sudden pressure changes as the reflections moved from the first to the second wedge. The different reflection processes predicted by the analysis, and the shock structures predicted by the shock polars have all been verified experimentally using shadowgraph and schlieren photographs. The shock waves which support the sudden pressure changes produced by some of the transitions and predicted by the shock-polar solutions, have been observed. In some cases these shocks are normal to the reflecting surface and in other cases they are regularly reflected shocks. The criteria to determine which of those configurations will occur, have not yet been established, but are the subject of continuing studies.

The authors gratefully acknowledge the helpful suggestions made by the participants of the 4th Mach Reflection Symposium in Tokyo and Sendai, and by their

colleagues at the Universities of Tohoku, Japan, Victoria, Canada, and Ben Gurion University of the Negev, Israel. The financial support received from DNA for supporting G.B.-D.'s sabbatical leave at the University of Victoria is gratefully acknowledged. The assistance received from Dr D. K. Walker in running the computer program for plotting the shock polars and his help in preparing this paper is gratefully acknowledged. We would like to thank Profesor M. Honda of the Institute of High Speed Mechanics, Tohoku University for his encouragement during the course of this study.

REFERENCES

BEN-DOR, G. 1978 UTIAS Rep. No. 232. University of Toronto, Toronto, Canada.

BEN-DOR, G. 1980 *Can. Aero. & Space J.* **26**, 98.

BEN-DOR, G., TAKAYAMA, K. & KAWAUCHI, T. 1980 *J. Fluid Mech.* **100**, 147.

COURANT, R. & FRIEDRICHS, K. O. 1948 *Hypersonic Flow and Shock Waves*. Wiley-Interscience.

DEWEY, J. M. & MCMILLIN, D. J. 1985 *J. Fluid Mech.* **152**, 67.

DEWEY, J. M. & WALKER, D. K. 1975 *J. Appl. Phys.* **46**, 3454.

DEWEY, J. M., WALKER, D. K., LOCK, G. C. & SCOTTEN, L. N. 1983 *Shock Tubes and Waves* (ed. R. D. Archer & B. E. Milton), p. 144. New South Wales University Press.

GINZBURG, I. P. & MARKOV, Y. S. 1975 *Fluid Mech. Sov. Res.* **4**, 167.

HEILIG, W. H. 1969 *Phys. Fluids Suppl.* **12**, I154.

HENDERSON, L. F. & LOZZI, A. 1975 *J. Fluid Mech.* **68**, 139.

HENDERSON, L. F. & WOOLMINGTON, J. P. 1983 *Shock Tubes and Waves* (ed. R. D. Archer & B. E. Milton), p. 160. New South Wales University Press.

HORNUNG, H. G., OERTEL, H. & SANDEMAN, R. J. 1979 *J. Fluid Mech.* **90**, 541.

ITOH, S., OKAZAKI, N. & ITAYA, M. 1981 *J. Fluid Mech.* **108**, 383.

JONES, D. M., MARTIN, P. M. & THORNHILL, C. K. 1951 *Proc. R. Soc.* A **209**, 238.

KAWAMURA, R. & SAITO, H. 1956 *J. Phys. Soc. Japan* **11** (5), 584.

VON NEUMANN, J. 1963 *Collected Works*, vol. 6. Pergamon.

TAKAYAMA, K. & BEN-DOR, G. 1985 *AIAA J.* **23**, 1853.